

Grain-size segregation and levee formation in geophysical mass flows

C. G. Johnson,^{1,2} B. P. Kokelaar,³ R. M. Iverson,⁴ M. Logan,⁴ R. G. LaHusen,⁴ and J. M. N. T. Gray¹

Received 8 August 2011; revised 18 November 2011; accepted 6 December 2011; published 22 March 2012.

[1] Data from large-scale debris-flow experiments are combined with modeling of particle-size segregation to explain the formation of lateral levees enriched in coarse grains. The experimental flows consisted of 10 m³ of water-saturated sand and gravel, which traveled ~80 m down a steeply inclined flume before forming an elongated leveed deposit 10 m long on a nearly horizontal runout surface. We measured the surface velocity field and observed the sequence of deposition by seeding tracers onto the flow surface and tracking them in video footage. Levees formed by progressive downslope accretion approximately 3.5 m behind the flow front, which advanced steadily at ~2 m s⁻¹ during most of the runout. Segregation was measured by placing ~600 coarse tracer pebbles on the bed, which, when entrained into the flow, segregated upwards at ~6–7.5 cm s⁻¹. When excavated from the deposit these were distributed in a horseshoe-shaped pattern that became increasingly elevated closer to the deposit termination. Although there was clear evidence for inverse grading during the flow, transect sampling revealed that the resulting leveed deposit was strongly graded laterally, with only weak vertical grading. We construct an empirical, three-dimensional velocity field resembling the experimental observations, and use this with a particle-size segregation model to predict the segregation and transport of material through the flow. We infer that coarse material segregates to the flow surface and is transported to the flow front by shear. Within the flow head, coarse material is overridden, then recirculates in spiral trajectories due to size-segregation, before being advected to the flow edges and deposited to form coarse-particle-enriched levees.

Citation: Johnson, C. G., B. P. Kokelaar, R. M. Iverson, M. Logan, R. G. LaHusen, and J. M. N. T. Gray (2012), Grain-size segregation and levee formation in geophysical mass flows, *J. Geophys. Res.*, 117, F01032, doi:10.1029/2011JF002185.

1. Introduction

[2] Scientific documentation of depositional levees bordering the paths of debris flows and avalanches dates back more than a century [e.g., *Stiny*, 1910; *Heim*, 1932], and modern work on geophysical mass flows, including debris flows, snow avalanches and pyroclastic flows adds quantitative rigor to such observations [e.g., *Conway et al.*, 2010; *Bartelt and McArdell*, 2009; *Hoblitt*, 1986; *Calder et al.*, 2000]. Early eye-witness accounts of the levee-formation process include that of *Sharp and Nobles* [1953], who noted that levees formed as resistive, coarse-grained debris-flow snouts were shouldered aside by advancing finer-grained debris. Thus, scientific observers have long recognized the important role of heterogeneous debris-flow architecture during levee formation: high-friction, coarse-

grained snouts are displaced laterally by subsequent finer material that has lower friction. Implicitly this view also recognizes the importance of grain-size segregation, which contributes to the heterogeneous flow architecture.

[3] Pioneering quantitative work on debris-flow mechanics and levee formation, especially that by *Johnson* [1965, 1970] and *Johnson and Rodine* [1984], acknowledged the heterogeneous character of debris flows but sought to simplify the phenomenon to make it more amenable to analysis. Thus, Johnson adopted a homogeneous Bingham model as a substitute for a more complicated “Coulomb-viscous” model of debris-flow rheology. Interpretations based on the Bingham model [e.g., *Rowley et al.*, 1981; *Wilson and Head*, 1981; *Mangold et al.*, 2010] assume that levees form as a consequence of the material yield strength, independent of the influences of internal flow dynamics or heterogeneous flow architecture.

[4] Evidence contradicting the Bingham model of levee formation comes both from field observations [*Sharp and Nobles*, 1953] and from reproducible large-scale experiments involving flows of ~10 m³ of heterogeneous, water-laden debris [i.e., *Iverson*, 1997; *Major*, 1997; *Major and Iverson*, 1999; *Iverson et al.*, 2010]. In these experiments, coarse grains (i.e., gravel) became concentrated at flow

¹School of Mathematics and Manchester Centre for Nonlinear Dynamics, University of Manchester, Manchester, UK.

²Now at Department of Mathematics, University of Bristol, Bristol, UK.

³Department of Earth Sciences, University of Liverpool, Liverpool, UK.

⁴Cascades Volcano Observatory, U.S. Geological Survey, Vancouver, Washington, USA.

fronts as a result of size segregation, and levee formation appeared to involve the same shouldering aside of coarse snout debris noted by *Sharp and Nobles* [1953]. A key aspect of the process, well-documented with basal pore pressure and normal stress data, was the persistence of a nearly liquefied, low-strength state of fine-grained debris in the channelized flow interior. This mobile core material advected some of its downstream momentum into the resistive, coarse-grained snouts, thereby providing motive force to drive the snouts forward and produce the “shouldering” effect. In debris flows, it is the higher pore fluid diffusivity of the coarse-particle front that allows the high pore pressures generated in large-scale flows to dissipate [*Iverson*, 1997] and results in the bouldery head having greater frictional resistance to motion than the shearing dispersion behind it [*Major and Iverson*, 1999]. The evolving particle-size distribution within the flow therefore plays a crucial role in determining the local flow mobility.

[5] The presence of a flow head with greater resistance to motion than the material behind can result in a transverse flow-front instability [*Pouliquen et al.*, 1997; *Pouliquen and Vallance*, 1999] that causes a uniform advancing flow front to ‘finger’, that is, to split into a number of adjacent levee-channeled flows. Many aspects of this process remain poorly understood; for example, we do not know the mechanism that defines the characteristic width of the resulting lobate deposits, nor what controls the relationship between the width and height of levee-channeled flows, or how the overall runout distance may be increased by the spontaneous lateral constriction. *Félix and Thomas* [2004] suggest relationships between the geometry of the deposit and the height and velocity of the parent flow based on laboratory experiments, but deeper understanding of the mechanisms is needed to be able to anticipate large-scale flow behavior. This paper uses quantitative measurements of large-scale flows and their resulting deposits to identify particle-size segregation and transport as key levee formation mechanisms.

[6] When a mixture of large and small grains avalanches downslope it is well known that the particles segregate to develop an inversely graded (upward coarsening) particle-size distribution [*Bagnold*, 1954; *Middleton*, 1970; *Middleton and Hampton*, 1976]. In a sheared mixture that is able to dilate, the segregation occurs by the combination of kinetic sieving and squeeze expulsion [*Savage and Lun*, 1988; *Vallance and Savage*, 2000]. These processes describe the downward percolation of small particles, which are more likely than the larger grains to drop into spaces that open up beneath them, and the return flow of large particles toward the surface. Considerable progress has recently been made in accurately modeling segregation in bi-disperse avalanches using relatively simple models [e.g., *Savage and Lun*, 1988; *Dolgunin and Ukolov*, 1995; *Gray and Thornton*, 2005; *Gray and Chugunov*, 2006; *Thornton and Gray*, 2008; *Shearer et al.*, 2008; *Gray and Kokelaar*, 2010a, 2010b] that can predict the evolution of the size distribution in laboratory experiments [*Golick and Daniels*, 2009; *Wiederseiner et al.*, 2011].

[7] In geophysical mass flows, mechanisms other than kinetic sieving and squeeze expulsion may drive and modulate particle segregation. In high-concentration parts of pyroclastic flows, large pumice fragments may segregate upwards because they are positively buoyant [*Sparks*, 1976;

Branney and Kokelaar, 2002]. Segregation may be hindered by both a wide distribution of grain sizes [*Gray and Ancey*, 2011] and by the presence of interstitial fluids that reduce the density difference between particles and fluid and introduce viscous effects [*Vallance and Savage*, 2000; *Thornton et al.*, 2006].

[8] The segregation of large particles to the flow surface, where the velocity is greatest, results in their preferential transport to the flow front. Here, they may pass directly over the front and be buried by following material. Once buried, large particles can again segregate upwards through the flow, allowing them to recirculate near the flow front [*Pouliquen et al.*, 1997]. This process results in the formation of resistive bouldery flow fronts, as well as finer-grained tails, during the motion of geophysical mass flows.

[9] Some insights into the evolving particle size distribution can be obtained from the two-dimensional bi-disperse experiments of *Gray and Ancey* [2009], which showed that a coarse-rich flow front was connected to an inversely graded avalanche behind it by a mixed region in which coarse particles segregate upwards and fine particles descend [*Thornton and Gray*, 2008]. *Gray and Ancey* [2009] observed that as additional large particles were transported to the head it did not grow in size, but instead deposited the additional large grains onto the substrate. We show in this paper that, in three dimensions, the transport of coarse particles to the flow front is balanced by the deposition of coarse particles in static lateral levees.

2. Methodology

[10] We use the U.S. Geological Survey (USGS) debris-flow flume [*Iverson et al.*, 2010] to study the effect of particle-size segregation on flow propagation and deposits. The flume consists of a straight concrete channel 95 m long, 2 m wide and 1.2 m deep, inclined at 31° to the horizontal (Figures 1 and 2). In the lowest 8.5 m, the slope transitions smoothly to 4° before the flume opens onto a planar concrete runout pad, 25 m long and inclined at ~2.4°. At 12.5 m below the top of the flume, two vertical doors 2 m high form gates of a hopper that allows water-saturated sediment to be held and released. The flume walls and runout area are smooth, but most of the length of the flume bed, between 6 m downslope of the hopper and 3.5 m upslope of the flume mouth, is roughened with bumps 16 mm high and spaced 50 mm apart. The large size of the flume is motivated by scale-dependent phenomena in debris flows: the effect of pore fluid pressure in natural debris flows is under-represented by geometrically similar small-scale experiments, whereas the effects of grain inertia, fluid yield strength and viscosity are over-represented at small scales. Since these scale-dependent phenomena may strongly influence the segregation and deposition processes central to our experiments, we use large-scale flows in which the nondimensional parameters governing the flow approach those found in natural flows [*Iverson et al.*, 2010], rather than bench-top laboratory experiments.

[11] We report the results of two duplicate experiments, run on 25th and 27th August 2009, which used initial charges of 10 m³ of water-saturated sand (0.0625–2 mm; 33%) and gravel (2–32 mm; 66%) with a trace of mud (<0.0625 mm). This mixture was called ‘SG’ by *Iverson et al.* [2010], who

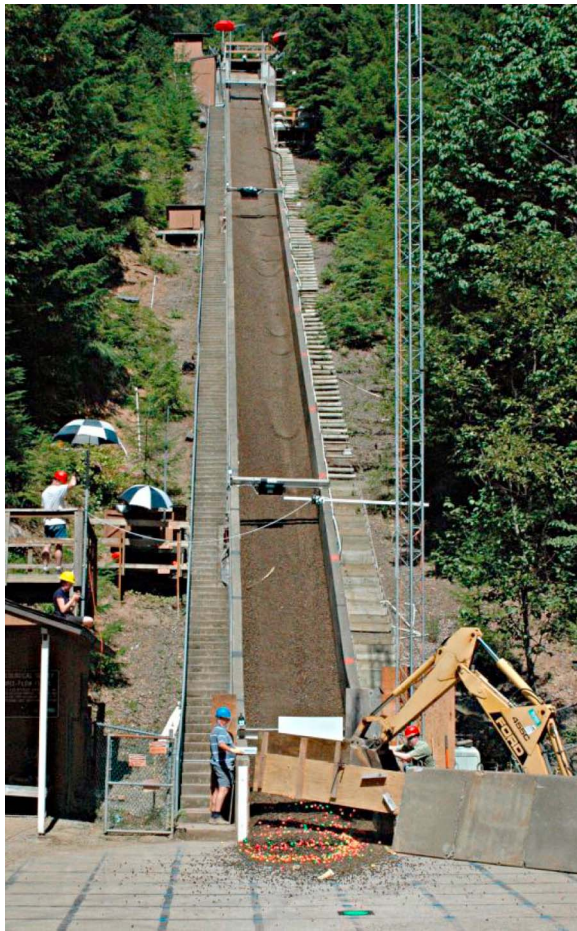


Figure 1. The USGS debris-flow flume, near Blue River, Oregon. This photo shows a debris flow ~ 14 s after it has been released from the hopper (top center). The head of the debris flow has reached the runout pad at the bottom of the flume, and has colored tracers on its surface which were dropped onto it as the flow exited the flume mouth. A wooden barricade, held above the flume mouth with the back-hoe of a tractor, allows the initial stages of the debris-flow runout to pass beneath it unimpeded. The diverter is dropped across the flume mouth once the bulk of the flow has passed, diverting the watery flow ‘tail’. Movies of this flow are shown in Animations 1 and 2.

give full details of the mixture properties and the experimental set up, and show that these experiments are reproducible. Reflecting our interest in the flow on the runout pad, in this paper $x = 0$ is at the lower end of the flume and the time $t = 0$ is defined to be when the flow first reaches $x = 0$ (Figure 2). We note that this contrasts with previous definitions of *Iverson et al.* [2010] in which the origin of x is at the flume headgates and $t = 0$ at the time of gate opening.

[12] When the flume hopper gates open, the wet sediment behind them collapses and accelerates down-slope, reaching the flume mouth in ~ 10 s (Figure 3 and Animation 1).¹ As the sediment mixture travels down the flume, it develops a

gravel-enriched snout followed by finer and wetter material; some coarse particles bounce far ahead of the snout. The debris then discharges onto the runout pad, forming an elongated deposit. In previous experiments [*Iverson, 1997; Major, 1997; Major and Iverson, 1999; Iverson et al., 2010*], after the debris flow had extended onto the runout area and deposited a well-formed leveed mound, a succession of water-rich roll-waves in the latter part of the flow overrode, eroded and partly buried the initial deposit, making it difficult to sample and interpret. To focus on the initial runout and deposition in our experiments, we truncated the flow shortly after the head discharged onto the runout pad and diverted most of the watery flow tail by dropping a reinforced plywood barrier obliquely across the flume mouth.

[13] During passage of the debris flows down the flume, continuous measurements of flow thickness, bed-normal stress and bed pore fluid pressure were made using the methodology described by *Iverson et al.* [2010], 32 m, 66 m and 80 m downslope from the hopper gates (Figure 3). The speed of propagation of the flow front, and the flow thickness and stresses at 32 m and 66 m, were nearly identical for the two experiments, and were very close to the mean behavior measured in previous experiments with similar experimental conditions [*Iverson et al., 2010, Figure 12*]. At 80 m below the gates (2.5 m upslope from the flume exit), the initial peaks in flow thickness and stresses, ~ 14 s after gate opening, were larger in the experiment of 27th August, indicating a more substantial flow head at this location in this experiment.

[14] To investigate the kinematics of the flow and deposition during the debris-flow runout, we measured the surface velocity field from overhead photograph sequences. Two Casio EX-F1 cameras mounted above the runout area on an overhead cable were triggered sequentially to record sequences of 105 images during the 2.5 s period when the flow front was between ~ 5 m and 10 m beyond the flume mouth. Photographs were taken at 60 frames per second for 1 s and 30 frames per second for the subsequent 1.5 s; the spatial resolution was approximately 3.5 mm per pixel. Surface flow velocities were calculated using Particle Tracking Velocimetry (PTV), which was facilitated by dropping 1600 brightly painted wooden tracers (2 cm \times 2 cm \times 2 cm cubes) onto the flow surface as it left the flume (Animation 2). The tracer cubes were painted four different colors, placed close-packed in rows on a board over the mouth of the flume (Figure 2) and dropped onto the flow surface steadily, in color sequence, over a period of ~ 3 s. Approximately 1000 colored tracer cubes and natural gravel particles were identified in each image, and the location of each tracked over ~ 25 adjacent frames. The velocity of each particle was calculated by taking a centered finite difference time derivative of its position, and the velocity field obtained by linearly interpolating the particle velocities on a Delaunay triangle mesh of the particle positions. The tracer cubes dropped onto the flow initially bounced over the surface, but settled onto the flow and accurately represented its surface velocity after traveling ~ 1.5 m downstream.

3. Flow Runout and Deposition

[15] After discharging from the flume, the debris flows of 25th and 27th August continued onto the runout pad for

¹Animations are available in the HTML.

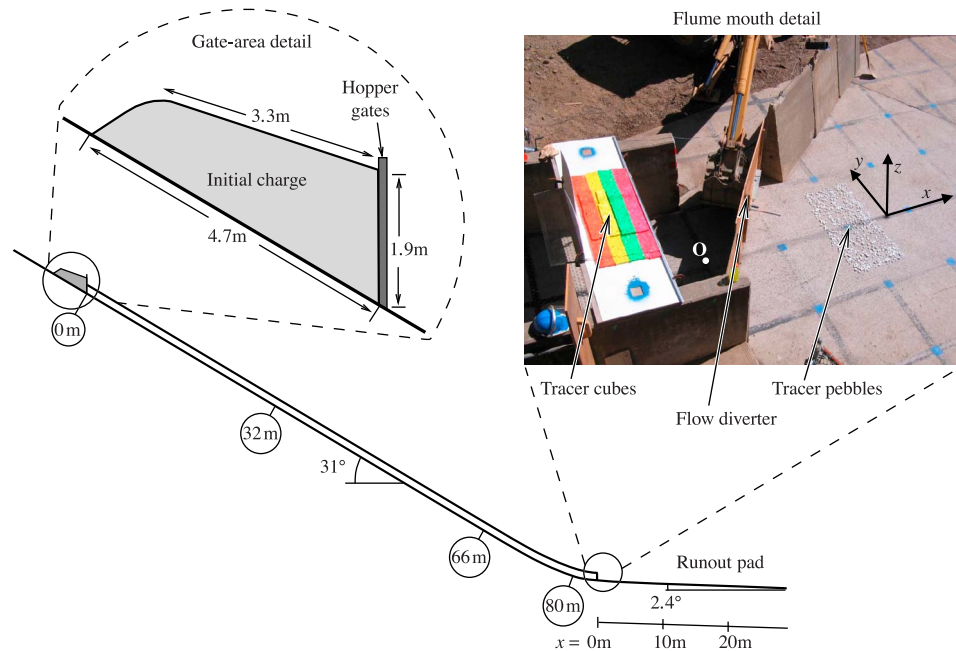


Figure 2. Longitudinal profile of the USGS debris-flow flume and runout pad, showing the location of the flow height, normal stress and pore pressure sensors, 32 m, 66 m, and 80 m below the headgates (after *Iverson et al.* [2010]). The left inset shows the shape of the initial 10 m^3 charge of sediment. The right inset is a photograph of the flume mouth area, showing the orientation of the xyz coordinate system. The origin O is located on the surface of the runout pad, at the center of the flume mouth. Grid squares are at 1 m intervals.

12 m and 9.5 m. These runout distances differ little from the runout lengths of 10.0 m, 10.3 m, 12.0 m and 16.5 m observed in similar experiments in which flows were not beheaded by the flow diverter [*Iverson et al.* 2010, Figure 17]. During the runout, both flows deposited continuously, as material near the front of the flow slowed in a flow ‘head’ region and deposited in levees that defined a flow channel of near-constant width (Figure 4a). Most of the runout distance was attained in the first 5 s after the flow exited the flume, when both the flow front and head propagated downstream at a near-steady velocity of 2.0 m s^{-1} . During this phase of the flow, the levees continuously accreted at the same rate of 2.0 m s^{-1} , approximately 3.5 m behind the front (Figure 4b). The deposit was formed in this near-steady flow regime, except for the most distal $\sim 3 \text{ m}$, which formed a bulbous snout as the flux of material at the flume exit waned and the flow front slowed dramatically (Figure 4c).

[16] The advancing flow head was thicker than the deposited levees (Figure 5), and exhibited the steep front and thin precursory flow seen in natural single-surge debris flows [*Sharp and Nobles, 1953; Pierson, 1986*]. During the experiments we observed approximately two traveling waves behind the resistive flow front; these waves progressed downstream at approximately the front propagation speed. The evolution of the amplitude and position of these waves (with respect to the flow front) caused temporal variation in flow head height, and repeated front steepening and collapse affected the size of the thin precursory surge ahead of the flow. However, these unsteady phenomena

caused only minor perturbation of the overall steady propagation of the flow front, as evidenced by the highly uniform width and height of the deposited levees.

[17] Tracing the path of particles through the flow head demonstrates the incremental formation of levees (Figure 6 and Animation 3). The marked particles in Figure 6 initially form two parallel lines in the central flowing channel, with particle 1 furthest downstream. Particles are first advected toward the flow front, then outwards into the levees where they deposit, resulting in a reversal of down-slope position; particle 1 is deposited furthest upslope. This reversal of longitudinal position is also evident from the color of the tracer cubes deposited in the levees (Figure 7).

[18] Only about half of the tracer cubes that were placed on the flow surface remained on the surface of the final deposit; the remainder were found buried within the deposit interior. Those that were initially near the flow margins remained on the surface and were advected onto the levee surface, whereas those nearer the flow centerline were transported to the flow front, overpassed and buried by subsequent material (Figure 8).

[19] At their full development, the levees occupied approximately half the flow width and the channelized flow between them was directed entirely down-slope (Figure 9a), with a rounded cross-slope velocity profile (variation of down-slope velocity with y) observed also in some natural debris flows [*Pierson, 1986*]. These features were typical of the regime of steady front propagation and levee formation since the channelized flow exhibited only slight temporal variation (Animation 4). At $t = 3.5 \text{ s}$ (the time shown in

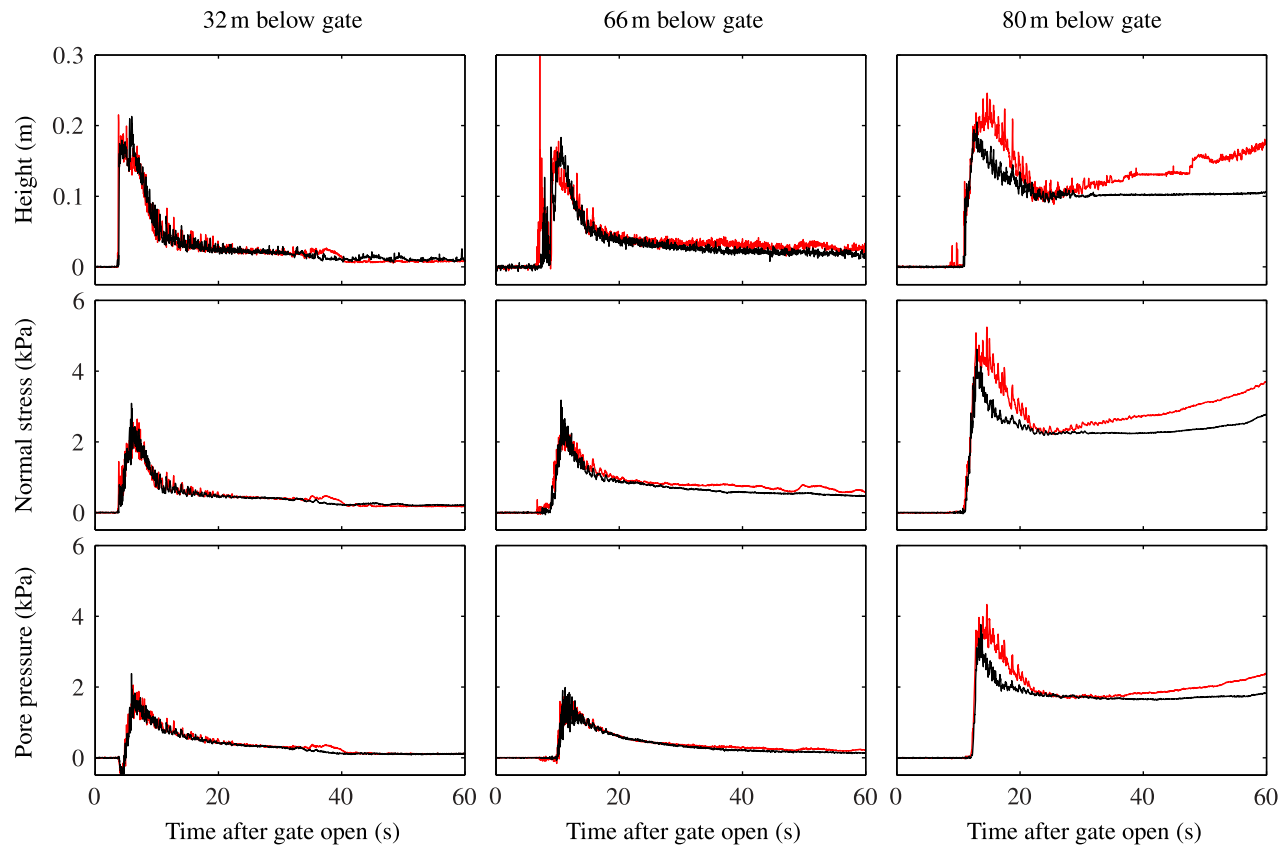


Figure 3. Flow depth, basal normal stress and basal pore pressure measurements for the experiments of 25th August (black) and 27th August (red). Measurements are taken at three locations: 32 m, 66 m, and 80 m downslope of the headgates. The time $t = 0$, at which the flow front leaves the mouth of the flume, occurs ~ 12.5 s after the gate opens. The relative increases in all quantities late in the 27th August flow merely reflect a greater proportion of the flow tail backing-up against the diverter, which was emplaced 16–18 s after gate opening, rather than being diverted to one side as occurred in the 25th August flow.

Figure 9a), the maximum downstream surface velocity was 6.1 m s^{-1} , with a variation of less than $\pm 2\%$ along the leveed section from $x = 1.5 \text{ m}$ to $x = 4.5 \text{ m}$. The cross-slope velocity profile and the levee width similarly exhibited only small streamwise variation; thus, upstream of the head, the levees and flow were largely independent of the downstream coordinate x .

[20] Within the flow head, material across the entire width of the flow was in motion, with the surface velocity close to the flow front almost uniformly 3 m s^{-1} , about $1.5\times$ faster than the propagation speed of the front. A transverse velocity component of $\sim 0.75 \text{ m s}^{-1}$ in the flow head advected particles away from the axis and toward the flow margins.

[21] Transverse and vertical shear rates were similar in the leveed channel (both of order 20 s^{-1}), indicating that horizontal stresses – commonly neglected in depth-integrated flow models – play an important role in the dynamics of levee-channeled debris flows [Denlinger and Iverson, 2004].

3.1. Flow and Deposition in a Moving Reference Frame

[22] The constant speed of propagation of the flow head and streamwise accretion of levees (Figure 4c), together with

the constant width and lack of streamwise variation of the levee-channeled flow behind the head (Figure 9a), indicate that the flow is best understood in a frame moving with the flow front, at the constant propagation speed of 2.0 m s^{-1} (Figure 9b and Animation 5). In this reference frame, the velocity field is steady and the flow margins are fixed, which implies that particle paths illustrated in Figures 6d and 8b coincide exactly with the surface streamlines. The correspondence of particle paths with streamlines in the moving frame means that the particles highlighted in Figure 6, which each start at the same y -location, all follow the same streamline through the flow head. As they slow and transition in the flow head from moving toward the flow front to being left behind by it, they reverse order. In Figure 9b, streamlines originating close to the central flow axis follow a path through the head and intersect the flow boundary. Streamlines originating farther from the flow axis curve back on themselves (corresponding to the flow being slowed to below the propagation speed of the front) and connect to a levee. These two surface flow patterns correspond to the two behaviors identified in Figure 8, where particles either reach the flow boundary and are overpassed by following material, or remain on the surface as they are advected into the levees.

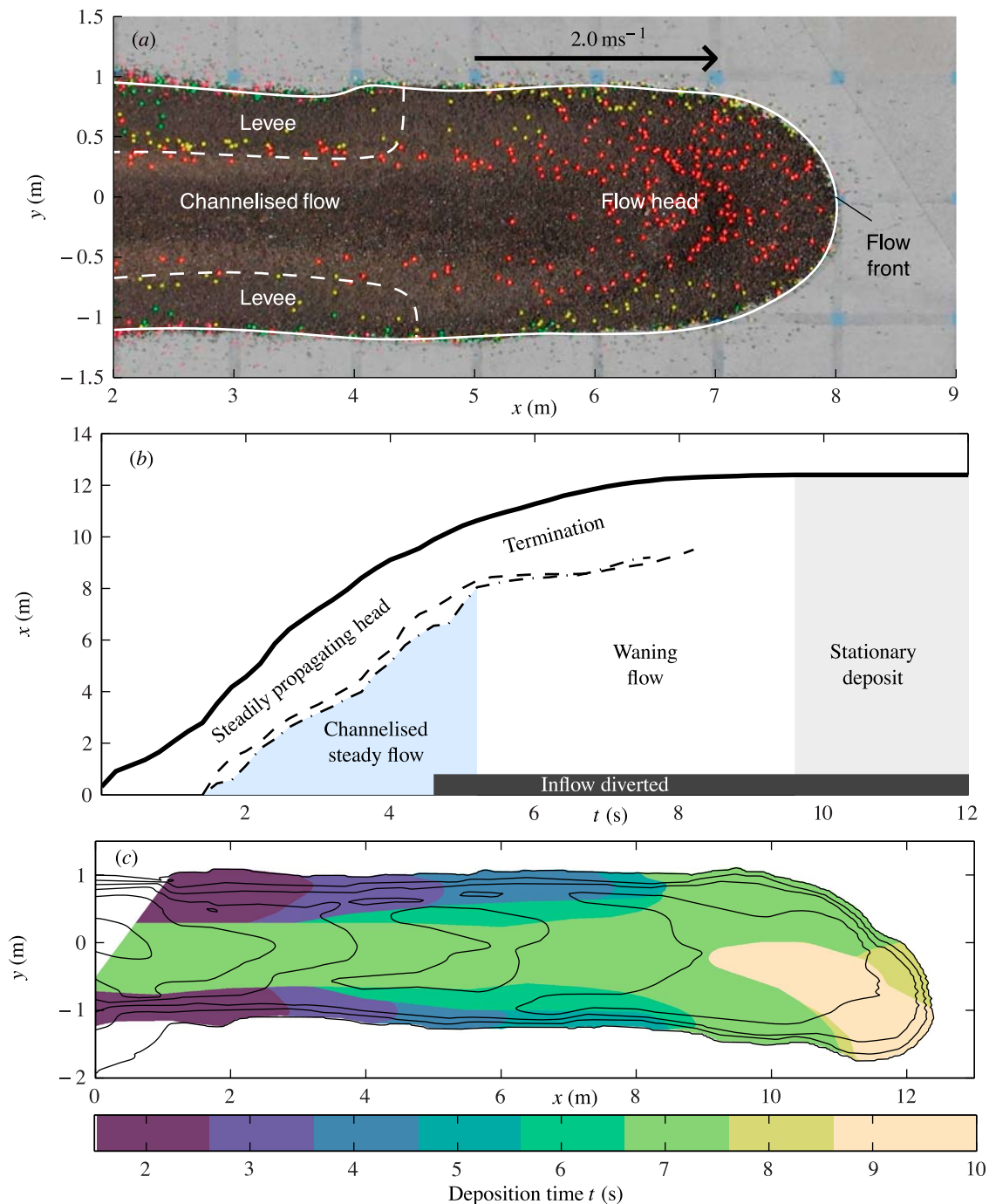


Figure 4. (a) Overhead view of the 25th August debris-flow runoff, 3.5 s after it first reached the flume mouth. The main features are the flow head, which forms the distal 3.5 m of the flow, and a channelized flow bounded by stationary levees that extend back to the flume. The flow head propagates at a steady velocity of $\sim 2.0 \text{ m s}^{-1}$, progressively extending the levees and the length of the channelized flow. (b) Downstream location of the flow front (solid line) and maximum downstream extents of left and right levees (dashed and dot-dashed lines respectively), as functions of time. (c) Timing of surface deposition, indicated by color, illustrates the streamwise accretion of levees. Contours show final deposit thickness, with 5 cm spacing.

3.2. Three-Dimensional Flow Model

[23] To understand the three-dimensional structure of the flow, a velocity profile is required to specify how the down- and cross-slope flow velocities vary with depth. While such

profiles are difficult to measure experimentally, we can infer something about them from observations of the surface velocity field. We construct a mathematical model in which the shape and velocity field of the flow are prescribed functions, chosen to match the observed shape and velocity

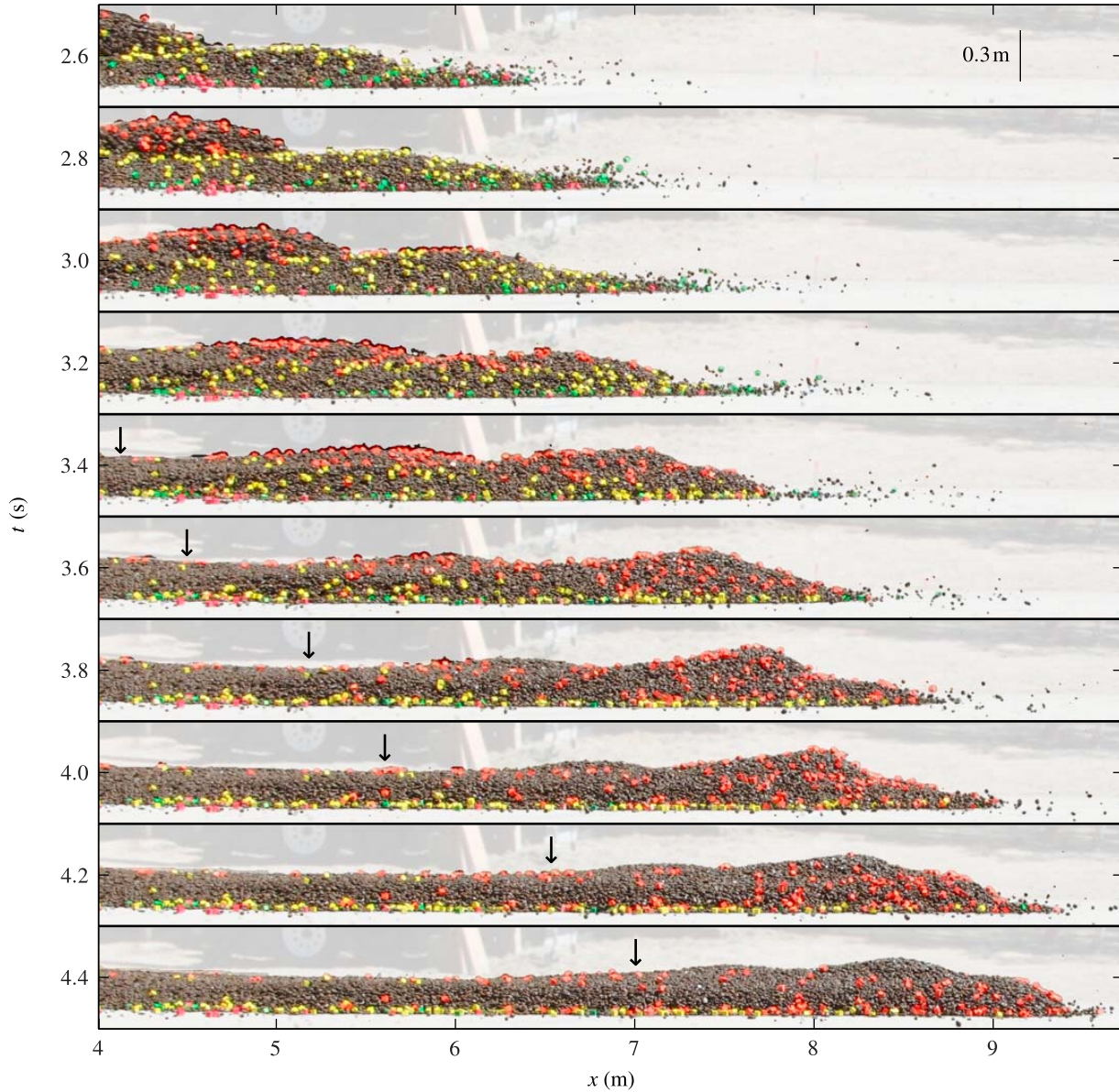


Figure 5. Time-sequence of side-view photographs of the August 25th debris-flow runoff. The arrow indicates the maximum downstream extent of the deposited stationary levee. The vertical scale of each photograph covers ~ 60 cm.

field of the experimental debris flows. Motivated by the experiments, we assume the flow is steady in a frame moving at the constant front speed. We use the coordinate system (x, y, z, t) (illustrated in Figure 2) in the stationary frame, and (ξ, y, z) in a frame moving with the flow front, where x is the down-stream coordinate in the stationary frame, y is the cross-stream coordinate, z the slope-normal coordinate, t is time, $\xi = x - u_F t$ is the down-stream coordinate in the moving frame and u_F is the front speed. The lack of a time coordinate in the frame moving with the flow front reflects the steady nature of the flow in this frame.

[24] The compressibility of the experimental debris flows is negligible because both water and particle constituents are incompressible, and the debris remains substantially

water-saturated throughout the duration of the flow. We therefore assume a divergence-free velocity field in the model, and denoting the flow velocity in the stationary frame by $\mathbf{u}(x, y, z, t) = (u, v, w)$, we obtain

$$\frac{\partial u}{\partial x} + \frac{\partial v}{\partial y} + \frac{\partial w}{\partial z} = 0, \quad (1)$$

which places a strong restriction on the possible velocity fields.

[25] In the stationary frame, the depth-averaged flow velocity $\bar{\mathbf{u}} = (\bar{u}, \bar{v})$ is defined by

$$\bar{u} = \frac{1}{h} \int_0^h u dz, \quad \bar{v} = \frac{1}{h} \int_0^h v dz, \quad (2)$$

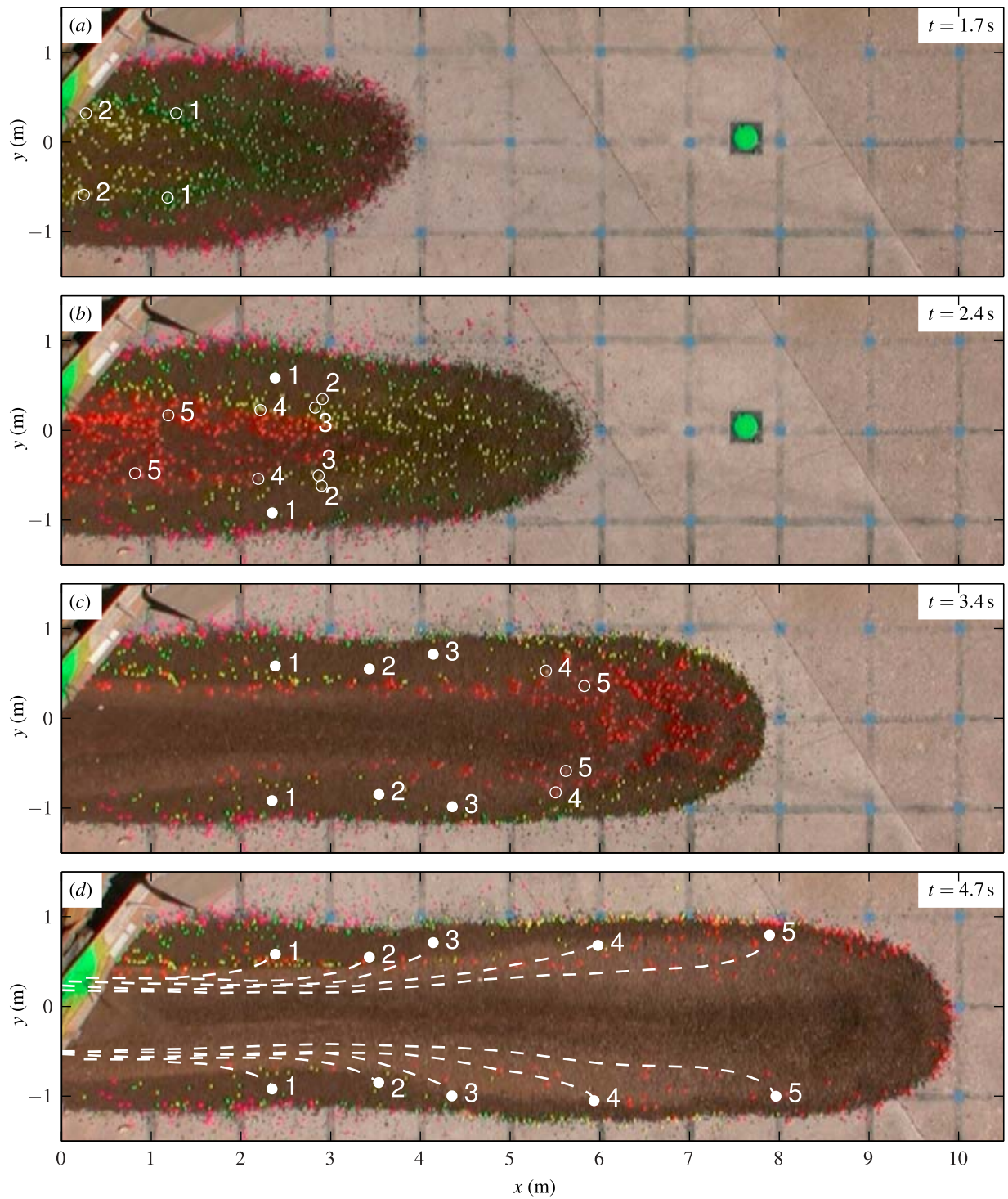


Figure 6. Overhead views of surface trajectories of particles in the August 25th experiment. Between each frame, the flow advances by 2 m. Moving particles are marked with open circles, and deposited particles with filled circles. (a) Particles marked 1 are farthest downstream in the flow, followed by particles 2–5 in sequence (3–5 out of frame). (b, c) As the flow progresses, those particles closest to the flow front are advected outwards and deposited. (d) The sequence of particles when deposited, is reversed from that in the flow, with particles marked 5 farthest downstream. An animated version of this figure is shown in Animation 3.



Figure 7. Oblique ground-level photograph of the August 27th experimental deposit, looking upslope from the deposit termination. Tracer cubes deposited on the surface lie on or near the levees at the flow margins, rather than in the central channel. The tracer cubes are deposited in colored bands, from orange cubes near the deposit termination (foreground), then yellow, then green, then pink cubes near the flume mouth. This pattern represents a reversal of the order in which the cubes were seeded onto the flow surface; the last cubes to be seeded onto the flow (orange), were deposited furthest from the flume mouth.

where h is the flow height. The depth-averaged velocity is linked to the flow height by the depth-averaged mass balance equation

$$\frac{\partial h}{\partial t} + \frac{\partial}{\partial x}(h\bar{u}) + \frac{\partial}{\partial y}(h\bar{v}) = 0, \quad (3)$$

obtained by integrating equation (1) in z and applying kinematic boundary conditions at the surface and base of the flow. This depth-averaged mass balance equation is a key part of shallow-layer avalanche and debris-flow models [Savage and Hutter, 1989; Gray *et al.*, 1999; Iverson and Denlinger, 2001; Gray *et al.*, 2003]. In the moving frame, the flow is steady and equation (3) reduces to

$$\frac{\partial}{\partial \xi}(h(\bar{u} - u_F)) + \frac{\partial}{\partial y}(h\bar{v}) = 0, \quad (4)$$

or, in the moving-frame depth-averaged velocity components $\bar{u}' = \bar{u} - u_F$, $\bar{v}' = \bar{v}$,

$$\frac{\partial}{\partial \xi}(h\bar{u}') + \frac{\partial}{\partial y}(h\bar{v}') = 0. \quad (5)$$

This divergence-free form allows the depth-averaged velocity to be defined through a stream function ψ [e.g., Batchelor, 1967], which satisfies

$$\frac{\partial \psi}{\partial y} = h\bar{u}', \quad \frac{\partial \psi}{\partial \xi} = -h\bar{v}'. \quad (6)$$

[26] We now construct empirical functions that approximate the shape and velocity field of the experimental debris

flow. In plan view, $y = \pm y_0(\xi)$ (for $\xi \leq 0$) describes the flow boundary, where

$$y_0(\xi) = W \sqrt{\tanh\left(-\frac{\xi}{W}\right)} \quad (7)$$

is a function that represents the rounded front and constant width channel. The half-width of the debris flow is given by the constant W , here set to 1 m to match the width of experimental flows. The flow depth is similarly modeled by the function

$$h(\xi, y) = \frac{H}{W} \left(\frac{y_0^{2n} - y^{2n}}{y_0^{2n-1}} \right), \quad (8)$$

where H is the maximum debris-flow depth of 25 cm and $n = 4$ is a constant which is chosen to reflect the observed height profile of the experimental debris flows (Figure 10a).

[27] The depth-integrated flow velocity is constructed through equation (6) using an empirical stream function

$$\psi(\xi, y) = \frac{HU}{W^2} \left(ky_0^2 - \frac{k}{2n+1} \frac{y^{2n+1}}{y_0^{2n-2}} - \frac{1}{2m+1} \frac{y^{2m+1}}{y_0^{2m-2}} + \frac{1}{2n+2m+1} \frac{y^{2n+2m+1}}{y_0^{2n+2m-2}} \right), \quad (9)$$

where the constant $m = 2$ reflects the observed velocity field in the debris-flow head, and $k = (2n+1)/((2m+1)(2n+2m+1))$. The constant U scales the flow velocity, and is here set to 2.3 m s^{-1} in order to reproduce the experimentally

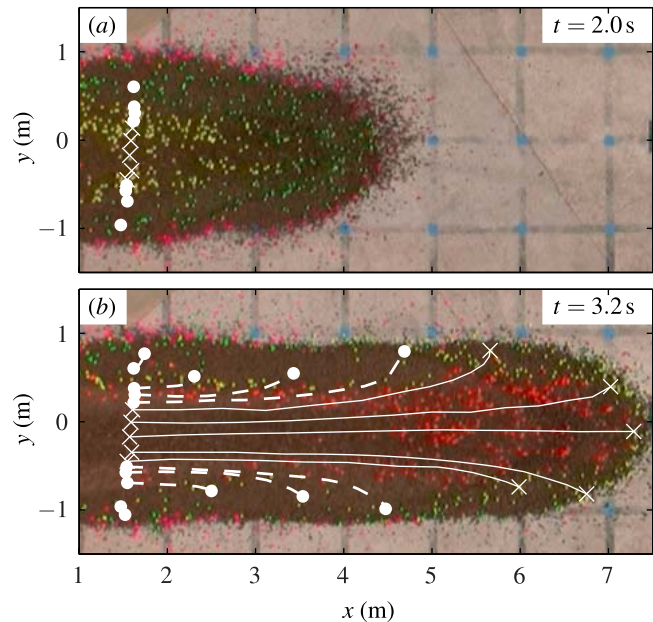


Figure 8. Surface and burial trajectories of particles in the August 25th experiment at (a) $t = 2.0 \text{ s}$ and (b) $t = 3.2 \text{ s}$. Particles close to the flow axis, marked with crosses (Figure 8a), are advected over the flow front and become buried (Figure 8b). Particles farther away from the flow axis, marked with filled circles, remain on the surface and are deposited on the surface of the levees.

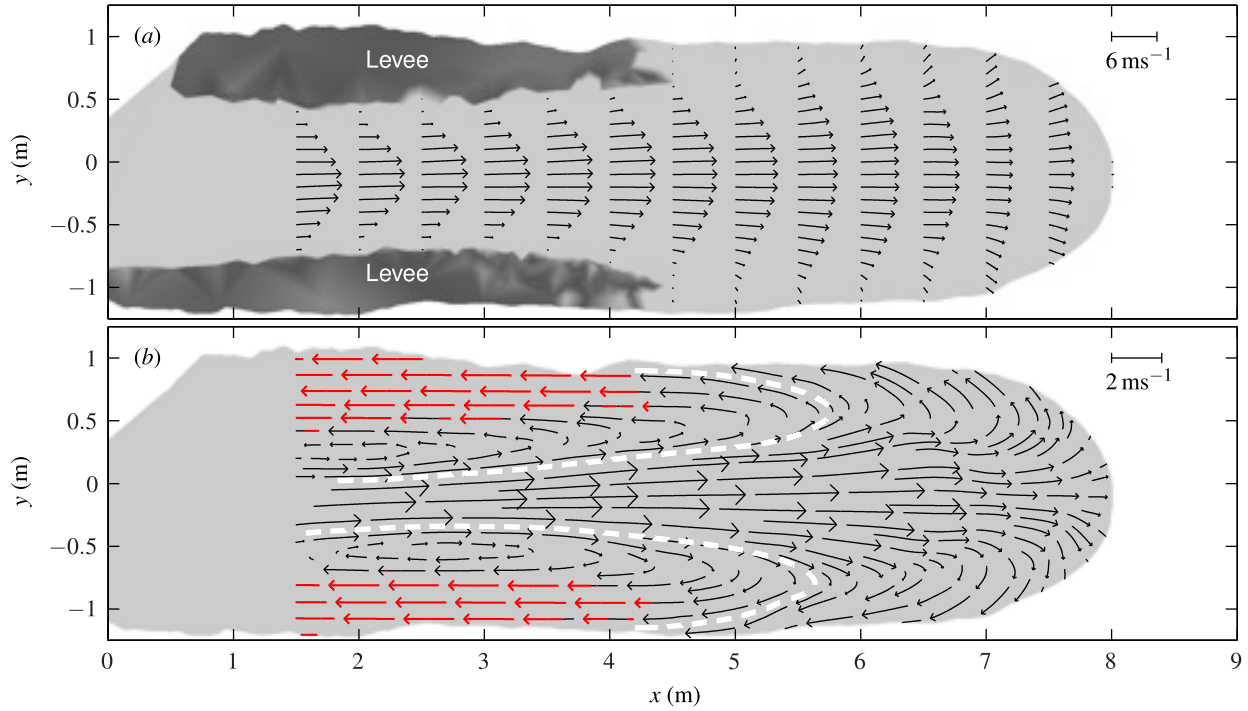


Figure 9. Surface velocities in the experiment of August 25th, 3.5 s after the flow reached the flume mouth (corresponding to the snapshot shown in Figure 4a). (a) The surface velocity field in a stationary frame. (b) Exactly the same velocity field, but in a frame moving at the speed of the head, at 2.0 m s^{-1} ; in this moving frame the velocity field is steady. Material that is effectively stationary, taken to be that moving at less than 4 cm s^{-1} , is indicated with darker shading in Figure 9a and with red arrows in Figure 9b. The white dashed line in Figure 9b demarcates surface particles near the center of the flow that reach the flow boundary and are buried, from those which remain on the surface and are advected onto the surface of the levees. Scale bars relate the length of arrows to the corresponding surface speed. The evolution with time of the flow surface speed is shown in Animation 4, and an overhead view of the runout in the frame moving with the flow front is shown in Animation 5.

observed front propagation speed of 2.0 m s^{-1} . Streamlines of the depth-integrated velocity field can be contoured in terms of ψ (Figure 10b).

[28] To determine a three-dimensional velocity field \mathbf{u} from the depth-integrated velocities $\bar{\mathbf{u}}$, the velocity profile is required. We determine the horizontal velocity components u and v through

$$(u, v) = f(z/h)\bar{\mathbf{u}}, \quad (10)$$

where $f(z/h)$ is an assumed velocity profile. The vertical component of velocity is then obtained by integrating the mass conservation equation in the moving frame with respect to z ,

$$w'(\xi, y, z) = - \int_0^z \frac{\partial u'}{\partial \xi} + \frac{\partial v'}{\partial y} dz'. \quad (11)$$

The velocity profile f , while difficult to observe directly in experiments, is constrained in several ways. For consistency with equation (2), we require that f satisfies

$$\frac{1}{h} \int_0^h f(z/h) dz = 1. \quad (12)$$

[29] Physically, we also expect the velocity to be greatest at the flow surface and decrease through the flow depth, constraining f to be a non-decreasing function. We consider a single-parameter family of profiles

$$f(z/h) = \left(\alpha + 2(1 - \alpha) \frac{z}{h} \right), \quad (13)$$

where the parameter α controls the amount of shear within the bulk of the flow ($0 \leq \alpha \leq 1$). When $\alpha = 1$, $(u, v) = \bar{\mathbf{u}}$, and a plug flow profile results, and when $\alpha = 0$, $(u, v) = 2\bar{\mathbf{u}}z/h$, representing linear shear with depth throughout the flow. With this choice of velocity profile, the horizontal components of the velocity in the moving frame are

$$u' = -u_F + (\bar{u}' + u_F) \left(\alpha + 2(1 - \alpha) \frac{z}{h} \right), \quad (14)$$

$$v' = \bar{v}' \left(\alpha + 2(1 - \alpha) \frac{z}{h} \right), \quad (15)$$

and the vertical velocity component, determined by equation (11), becomes

$$w' = u_F(1 - \alpha) \frac{z^2}{h^2} \frac{\partial h}{\partial \xi} - \left(\frac{\partial \bar{u}'}{\partial \xi} + \frac{\partial \bar{v}'}{\partial y} \right) \left(\alpha + 2(1 - \alpha) \frac{z}{h} \right) z. \quad (16)$$

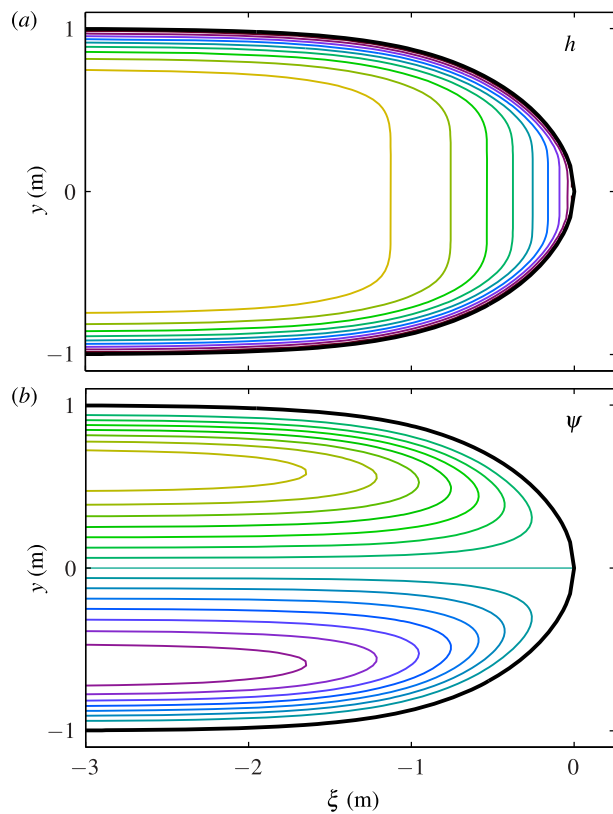


Figure 10. Functions chosen to model the debris-flow head. (a) Contours of h at intervals of 2.5 cm. (b) Contours of ψ which are streamlines of the depth-integrated velocity field (\bar{u}', \bar{v}') . The thick black line indicates the deposit margin at $y = \pm y_0(\xi)$.

The flow velocity in the frame moving with the flow front, denoted by $\mathbf{u}'(\xi, y, z) = (u', v', w')$, is defined by $\mathbf{u}' = \mathbf{u} - (u_F, 0, 0)$.

[30] The choice of velocity profiles (13) that combine linear shear and basal slip is made for simplicity. Other choices are possible, such as

$$f_n(z/h) = (2 - \alpha) \left[1 - \left(1 - \frac{z}{h} \right)^{1/(1-\alpha)} \right], \quad (17)$$

a family of non-linear velocity profiles with no slip and a shear maximum at the base of the flow, where α as before controls the shape of the profile, giving plug flow when $\alpha \rightarrow 1$ and simple linear shear when $\alpha = 0$. However, with the additional constraint on α that we infer from experimental measurements below, our results are insensitive to whether linear profiles with basal slip (equation (13)) or more complex profiles such as equation (17) are chosen.

[31] The motion of a particle through the model velocity field is given by

$$\frac{dr_x}{dt} = u, \quad \frac{dr_y}{dt} = v, \quad \frac{dr_z}{dt} = w, \quad (18)$$

where $\mathbf{r} = (r_x, r_y, r_z)$ is the particle location. As before, in the frame moving with the flow front, these particle paths coincide with streamlines of the three-dimensional flow.

[32] We present streamlines of the model debris flow for three different velocity profiles of the form given in equation (13), varying from plug flow ($\alpha = 1$) to uniform simple shear ($\alpha = 0$) (Figure 11). The columns show the assumed velocity profile, the surface velocities in the stationary frame, and surface streamlines (particle paths) in the frame moving with the flow front. The surface velocities shown in the second and third columns are directly comparable with the experimentally measured surface velocities shown in Figures 9a and 9b, respectively.

[33] The simplest velocity profile is that of uniform plug flow, shown in Figures 11a, 11b, and 11c. In this case, the flow in the x - y plane is equal to the depth-averaged flow velocity everywhere. As a result, the surface streamlines in Figure 11c coincide with the depth-averaged streamlines in Figure 10b and do not intersect the frontal boundary of the flow. No surface material is transported to the front and overpassed, and the surface velocity at the flow front is identical to the rate of flow propagation. This is qualitatively unlike the experimental surface velocity field shown in Figure 9b.

[34] Another possible flow profile is uniform simple shear, illustrated in Figures 11d, 11e, and 11f, where flow has a linear velocity profile. Almost all the surface streamlines in this case intersect the frontal boundary of the flow, corresponding to almost all the surface material dropping over the flow front and being buried, rather than being advected into the levee surfaces. Again, this behavior is unlike that in the experimental debris flows.

[35] A velocity profile where $\alpha = 0.5$ exhibits shear as well as basal slip (Figures 11g, 11h, and 11i). This profile matches the experimental observation that the surface velocity at the flow front is $1.5\times$ faster than the front propagation rate. Surface streamlines near the center of the channel reach the front, but toward the edges of the channel surface streamlines remain on the surface and are returned into the levees. We therefore infer that the velocity profile in the experimental debris flows is similar to that depicted in Figure 11d, in which shear with depth (variation of the downslope velocity with depth) is combined with some component of basal slip or a rapidly shearing region at the flow base. Video recordings of the advancing flow front, which show particles and tracer cubes on the flow surface being advected over the flow front and buried by the subsequent flow, provide additional direct evidence of shear in the flow.

[36] The velocity profile affects the three-dimensional transport of material through the flow head (Figure 12). Where u' is negative, material moves more slowly than the flow front (shaded pink in Figure 12). In the moving frame, this condition corresponds to the regions where material leaves the flow head. Conversely, where u' is positive (the corresponding unshaded regions in Figure 12), material enters the flow head. Solutions of the transport equation (18) give paths taken by particles that enter the head, flow through it, and leave it (in the region shaded pink). The incompressible and steady nature of the flow in the moving frame implies that the mass flux entering the head exactly matches the mass flux leaving it. This mass balance has important consequences for the particle size-

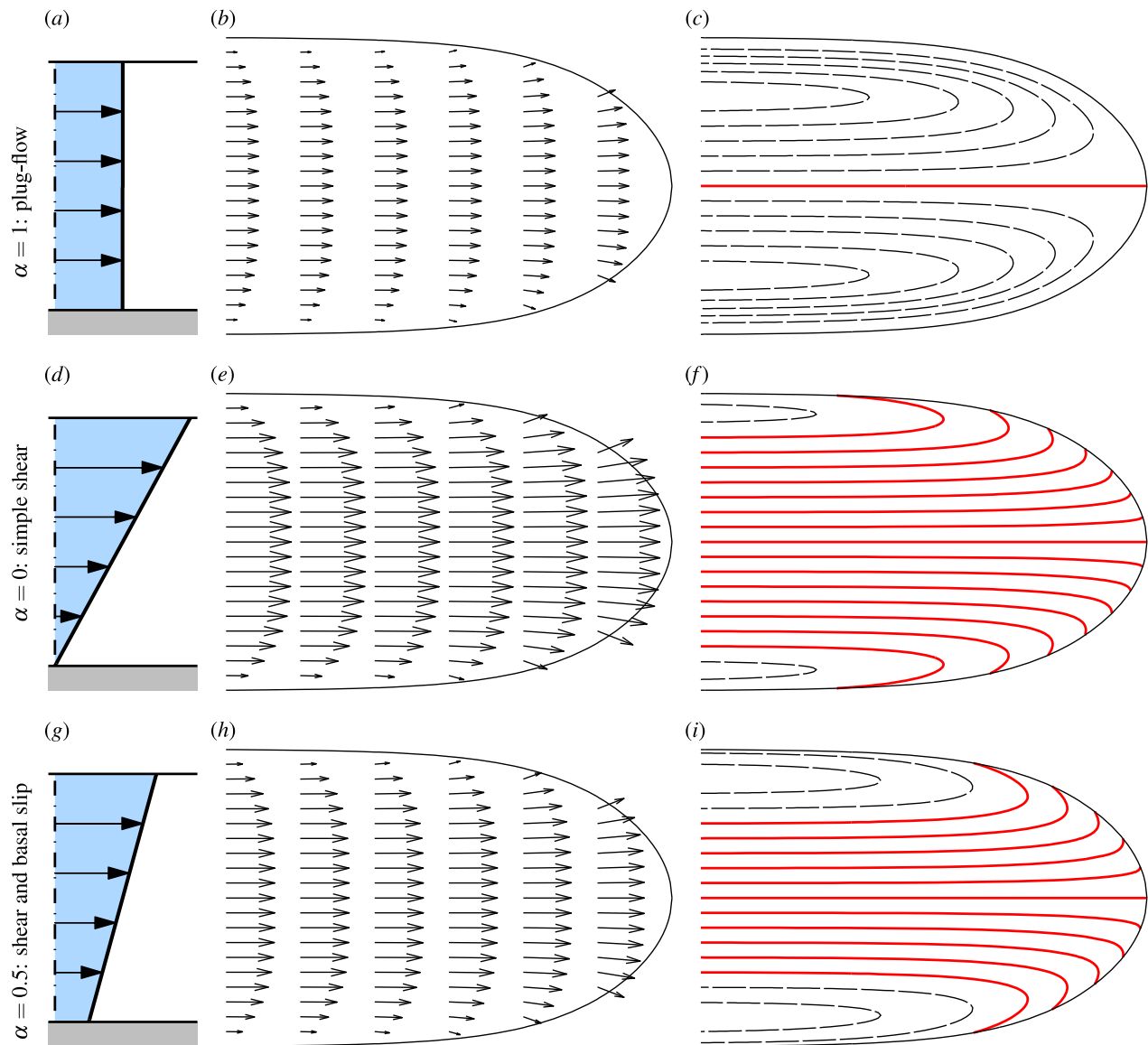


Figure 11. Assumed velocity profiles and resulting surface velocity fields in the debris-flow head, with the flow velocity field given by equations (14) and (15). The (a, d, and g) velocity profiles, (b, e, and h) surface velocity fields in the stationary frame, and (c, f, and i) streamlines in a frame moving with the flow front are each shown for three different velocity profiles. Figures 11a–11c illustrate plug flow ($\alpha = 1$), Figures 11d–11f illustrate simple shear ($\alpha = 0$), and Figures 11g–11i illustrate the combination of shear and basal slip that is inferred from the debris-flow experiments, where $\alpha = 0.5$. The surface velocities in the stationary frame are identical for all velocity profiles, up to a scaling factor. Solid red lines indicate the surface streamlines in the moving frame that reach the front of the flow; the proportion of material on the flow surface that reaches the flow front and is overpassed is strongly dependent on the extent of internal shear.

distribution in the flow head and is discussed further in section 7.

[37] Three-dimensional particle paths for the case of uniform plug flow show that material enters the head along the central axis of the flow, is advected outwards, and leaves along the flow margins (Figure 12a and Animation 6). Equations (16) and (18) imply that when there is no shear with depth, the relative height of a particle in the flow r_z/h remains constant.

[38] In the case of simple shear, (Figure 12b and Animation 7), material enters the head largely along the surface of the flow and leaves it in a layer at the base. There is very little transverse transport of particles; instead they are advected over the flow front and to the base of the flow in a ‘caterpillar-track’ motion.

[39] In the case of the experimentally inferred velocity profile (Figure 12c and Animation 8), particle paths combine transverse motion away from the flow centerline with

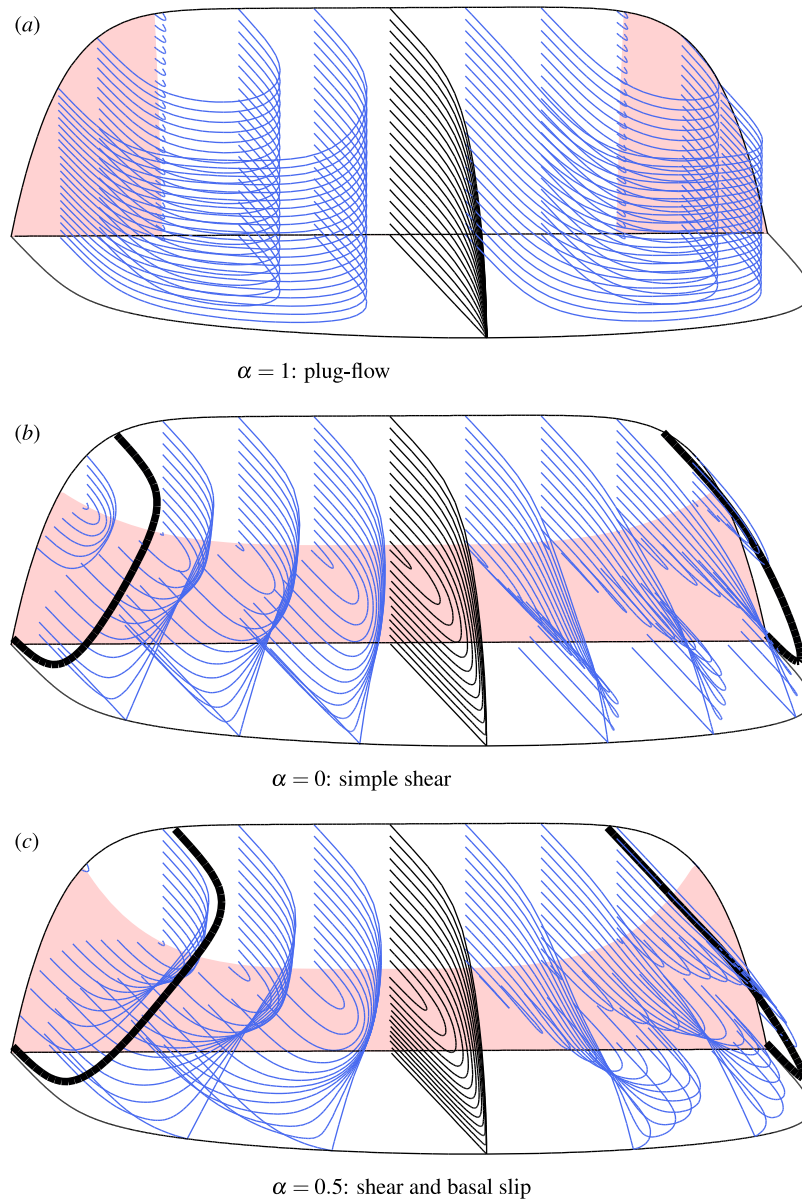


Figure 12. Computed three-dimensional particle paths within the flow head, with the flow velocity field given by equations (14), (15) and (16). Thick black lines indicate the boundary between particles that remain on the surface and those that reach the flow front and are buried. Pink shading indicates material that is moving downstream more slowly than (and therefore away from) the flow front; the corresponding unshaded regions indicate material moving toward the front, into the flow head. (a) In plug flow, all streamlines coincide with the depth-integrated streamlines, and material in the head is transported laterally from the central channel to the flow margins. (b) In the case of simple-shear, material from the top half of the flow, which is moving faster than the rate of propagation of the flow head, is transferred to the base of the flow as it passes over the flow front, with very little transverse motion. (c) At the intermediate velocity profile of $\alpha = 0.5$ present in the flume flow, material traveling through the flow head is both transported laterally within the flow head, and to the base of the flow as it passes over the flow front. The motion of particles on the surface and base of the flow, for the velocity profiles in Figures 11a–11c are shown in Animations 6–8, respectively.

vertical transport of particles over the flow front, from near the surface of the flow to near the base. This combination of transverse and vertical transport is a robust result; it is also found if we use a parabolic velocity profile, obtained from

equation (17) with the experimentally inferred value of $\alpha = 0.5$. Material leaves the flow head predominantly in two lateral levees, but also in a thin layer at the base of the flow. In the stationary frame, this material leaving the head is the

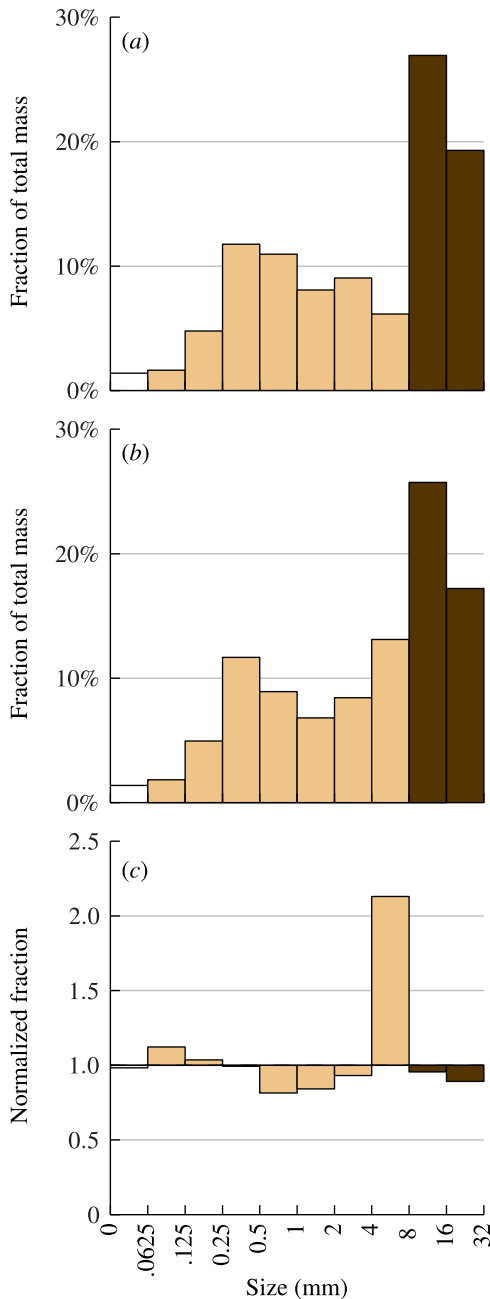


Figure 13. (a) Mean grain-size distribution of initial charge used in the August 25th experiment. (b) Mean grain-size distribution of initial charge used in the August 27th experiment. (c) Relative abundance plot showing the grain-size distribution of the August 27th initial charge normalized against that of the August 25th experiment. The axes for this histogram are the same as those used in the miniature plots in Figures 14 and 15, where histogram bars indicate enrichment (values >1) and depletion (values <1) of material in each grain-size class relative to the particle-size distribution of the relevant initial charge. Dark brown, tan and white shading denotes the classes of material identified as coarse, fine and very fine, respectively.

slowest-moving in the flow, indicating that it may deposit readily.

4. Deposit Granulometry

[40] Grain-size distributions were sampled from the initial charges (the material held in the hopper that was released to form a debris flow) and along four transects in the August 25th and August 27th deposits (Figures 13, 14, and 15). Three transverse transects and one axial transect each comprised three to six sample sites. At each sample site, a thin-walled steel tube 19 cm in diameter was inserted into the deposit and the material within it carefully excavated either from the top and bottom halves of the initial charge (in the August 25th deposit), or from the top, middle and bottom thirds (in that of August 27th).

[41] Sieve analyses yielded measures of dry mass in nine one- ϕ bins (each containing grains with effective diameters varying over a factor of two) between 0.0625 mm (1/16 mm) and 32 mm, and in one bin for particles smaller than 0.0625 mm. In order to highlight the evolved grain-size distributions that result from granular segregation, we normalize the deposit granulometric results against the granulometry of the initial charge. For each experiment, the grain-size distribution of the initial charge is taken to be the unweighted mean of the grain-size distributions of the four samples taken in the hopper. To normalize a sample, the proportion of dry mass in each size bin is divided by the corresponding proportion in the mean initial charge grain-size distribution. The initial charges of both experiments are bimodal (Figures 13a and 13b), with peaks at ~ 0.3 mm and ~ 12 mm corresponding to the constituent sand and gravel components respectively. The initial charges from the two experiments are generally similar (that is, the relative abundances are close to unity), although in samples taken from the August 27th charge the 4–8 mm particles are roughly doubled in abundance ($\sim 12\%$ as opposed to $\sim 6\%$, Figure 13c). This difference may be due to sampling error, or it may be representative of the whole initial charge; in either case, the grain-size distribution of the deposits indicates that particle-size segregation played a very similar role in both flows. In both deposits, samples typically indicate either a strong depletion of fine material or a grain-size distribution similar to the initial charge, suggesting that the deposits overall are fines-depleted. This is simply due to the use of the flow diverter, which prevented much of the fine-sediment-laden flow tail from reaching the deposit on the runoff pad.

[42] The relative abundances of size fractions sampled from flow deposits (Figures 14 and 15) show that in general there is coherence across a range of neighboring size bins, such that it seems justified to discuss three general classes of grains. We distinguish: *coarse* particles, from 8–32 mm; *fine* particles, from 0.0625–8 mm; and *very fine* particles, <0.0625 mm. The coarse and fine fractions correspond generally, but not exactly, to the two peaks of the bimodal particle-size distribution of the initial charge (Figure 13); the smallest gravel particles (of diameter 2–8 mm) segregate in the same manner as the sand and so are classified as fine. The very fine particles comprise less than 2% of the initial

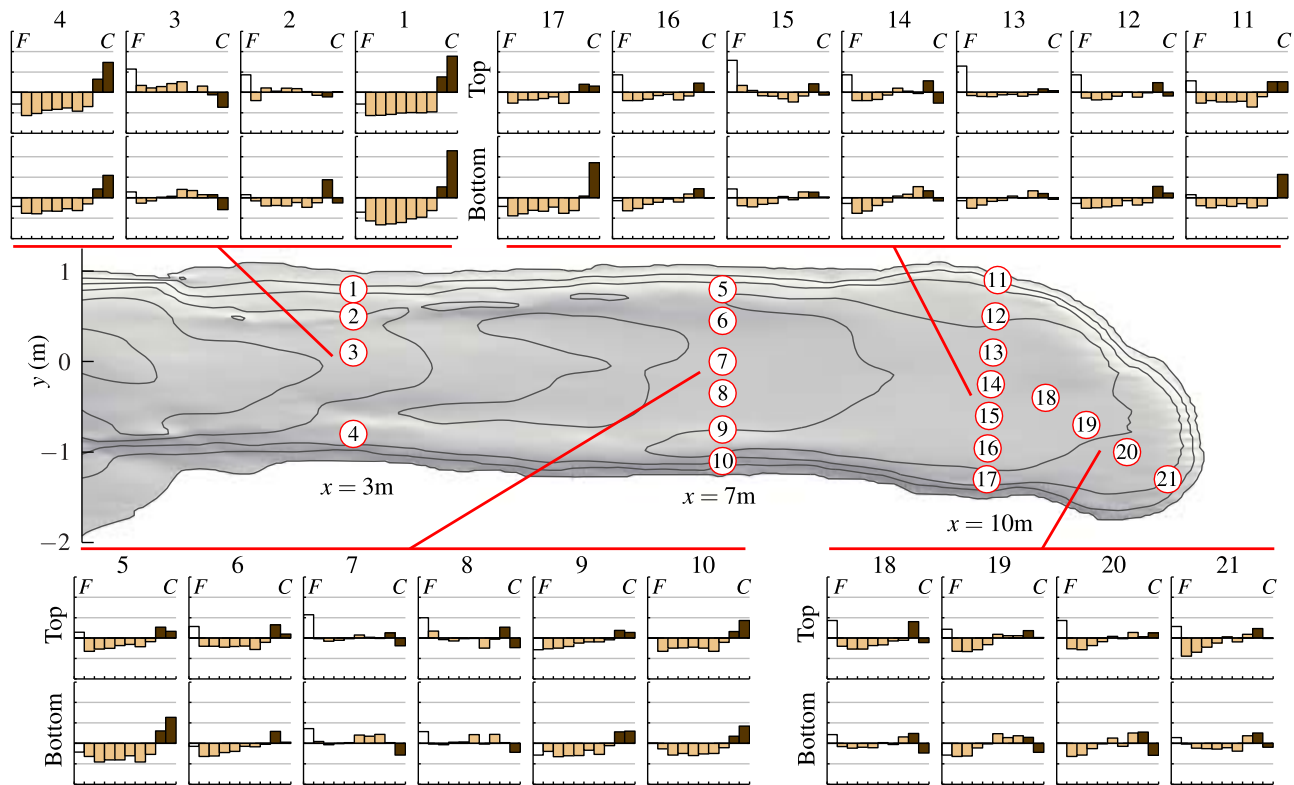


Figure 14. Relative abundance plots of deposit granulometry in the 25th August experiment. Axes for the plots are as for Figure 13c: coarse material (C) is to the right and fine material (F) to the left. Bars above the centerline indicate enrichment and those below the centerline indicate depletion. Contours show deposit thickness, with 5 cm spacing.

charge, so we concentrate on the relative abundances of the coarse and fine classes.

[43] In the proximal transect (at $x = 3$ m) of the August 25th deposit (Figure 14), coarse material is strongly enriched and fine material is depleted to approximately half of its initial concentration throughout the outer parts of the levees (sample sites 1 and 4). At the center of the leveed channel (site 3), the size distribution is closer to that of the source material, with a consistent relative depletion of the largest particles ($d > 16$ mm); no overall size grading is evident. At site 2, the basal enrichment of coarse and depletion of fine is taken to reflect the inner lower flank of the levee. These relationships are evident in the medial and distal transects ($x = 7$ m and $x = 10$ m). Overall, the deposit shows a proximal to distal progressive loss of the coarsest particles (16–32 mm).

[44] Similarly, the August 27th deposit (Figure 15) exhibits strong relative enrichment of coarse particles and corresponding depletion of fine ones in the levees. The relative enrichment of the coarsest particles in the levees is most marked at the top and bottom, with less enrichment in the middle. Samples nearer the deposit axis at $x = 2$ m and $x = 6.5$ m (sites 23 and 26) intersect levee material in the lower two thirds and at both of these sites the overall vertical organization is normal (coarse-tail) grading. At the center of the leveed channel in these transects, the deposits (sites 24 and 27) show slight coarse depletion but otherwise

no strong or consistent departures from the source material concentrations of coarse and fine particles.

5. Segregation and Recirculation

[45] In the August 27th experiment, ~ 600 pebbles with average diameter of ~ 20 mm, typical of the largest class of particles in the initial charge, were painted white and placed in a rectangular patch no more than one particle thick on the runout area, 2 m from the exit of the flume (Figure 2). As the debris-flow front advanced over the tracer pebbles, they were incorporated into the buried material, and thereafter reflected the paths of those large particles that reached the flow front and were overpassed at $x \approx 2$ m. The deposit was gradually removed by trowel, so as to reveal the plan view position and height of the pebbles (Figures 16 and 17).

[46] The tracer pebbles occupied a horseshoe-shaped region in the deposit (Figure 16), becoming progressively elevated and dispersed throughout the deposit down-stream. Pebbles transported less than 3 m were clustered in two parallel bands along the inner sides of the levees, with a complete absence of pebbles in the center of the channel. Those transported more than 3 m were elevated to around 12 cm above the deposit base, mainly in a broad zone centered on the flow axis, with few pebbles within 0.5 m of the deposit margin. The height attained by the tracer pebbles shows a clear increase with downstream distance, most

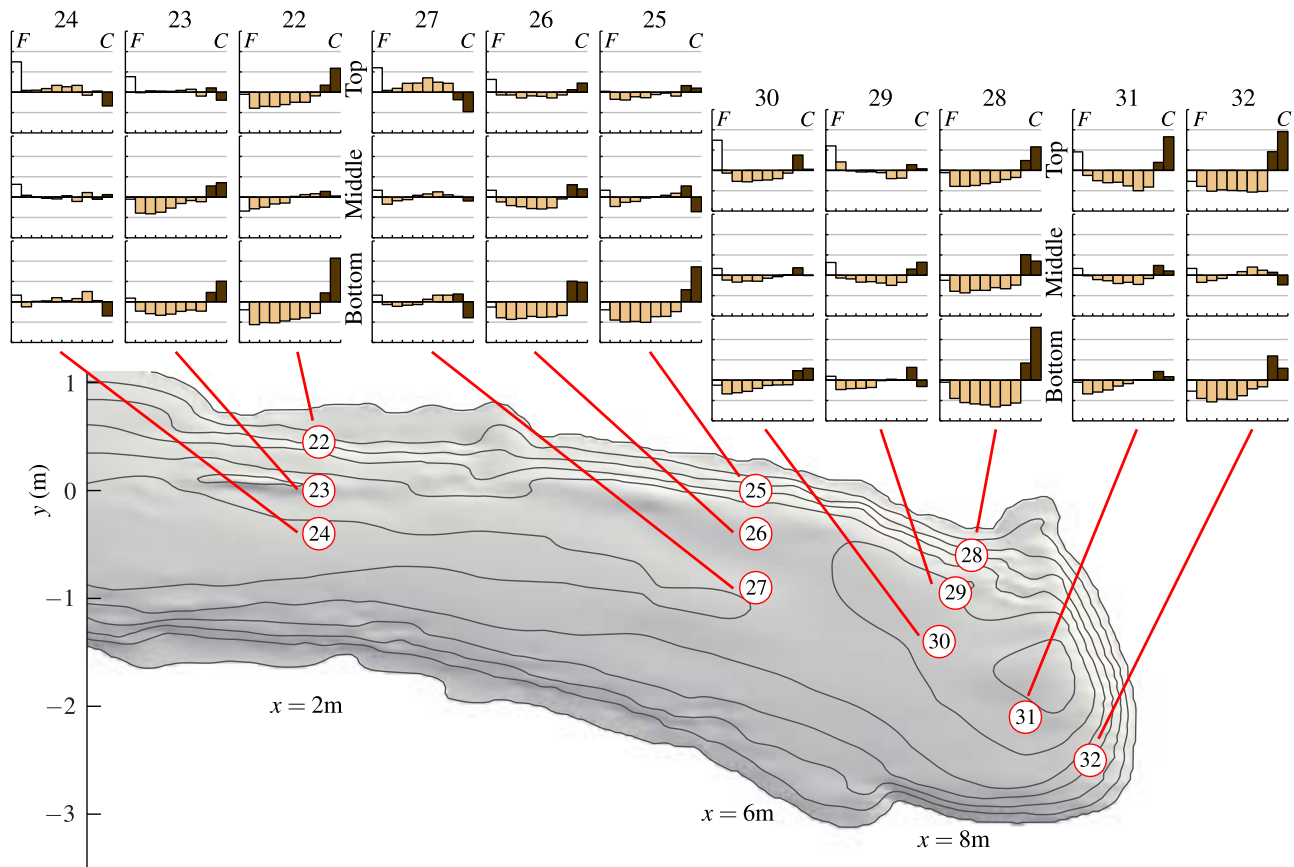


Figure 15. Relative abundance plots of deposit granulometry in the 27th August experiment. Axes for the plots are as for Figure 13c: coarse material (C) is to the right and fine material (F) to the left. Bars above the centerline indicate enrichment and those below the centerline indicate depletion. Contours show deposit thickness, with 5 cm spacing.

marked between 3.5 m and 5 m downstream from the flume exit. This positioning reflects a maximum rise of 15 cm in ~ 2.7 m of transport, or a streamwise climb angle of $\sim 3^\circ$. Between 5 m and 8.8 m downstream, where the most distal tracer pebble was located, the pebbles were distributed approximately uniformly in height within the bottom two-thirds of the deposit, ≤ 17 cm above the base. No tracers occurred in the uppermost 5 cm of the deposit and very few within 10 cm of the top surface.

[47] The downstream increase in tracer elevation provides evidence for size-segregation during runout of the debris flow. The possibility that the tracer pebbles reached a pre-existing deposited region and were then raised above the runout pad through ‘ramping’ (rolling up the inclined surface of a deposited region) is not consistent with their path through the flow head, from their introduction at the flow front to deposition in the progressively accreting levees. The typical rise velocity of the segregating pebbles can only be estimated since the time of deposition of particles in the interior of the flow is not known. However, videos of the flow indicate that deposition of levees occurs rapidly throughout the flow depth, and so the deposition time of particles in the levees is close to the stopping time of the surface material at that point. The tracer pebbles were overridden between $t = 1.1$ s and $t = 1.5$ s, and the deposition of the levee surface at $x = 5$ m, where particles reached

15 cm above the base, occurred at $t = 3.5$ s. This indicates a maximum rise rate of $6.3\text{--}7.5$ cm s^{-1} . Since tracer pebbles in the levee near $x = 5$ m were distributed quite uniformly between ground level and 15 cm above the runout pad, a typical rise rate is about half of the maximum rate, or ~ 3.5 cm s^{-1} .

6. Segregation and Transport Model

[48] Particle size-segregation, shear with depth and overpassing of material at the flow front lead to a net transport of coarse and fine particles to different locations in the flow and deposit. We now combine the velocity field of the flume runout inferred in section 3.2 with a simple model for particle segregation in a bi-disperse mixture (one composed of grains of two distinct sizes) proposed by *Gray and Thornton* [2005] to predict the distribution of large and small particles throughout the flow. We relate this distribution to observed grain-size distributions sampled from the deposit. The bi-disperse model describes the segregation of only two species of particles, whereas the experimental debris flows contain a continuous range of particle sizes. However, the bimodal distribution of the initial charge and the coherence of enrichment or depletion across neighboring size bins indicates that this bi-disperse segregation model may be applied to the flume runout, with coarse (8–32 mm) and fine

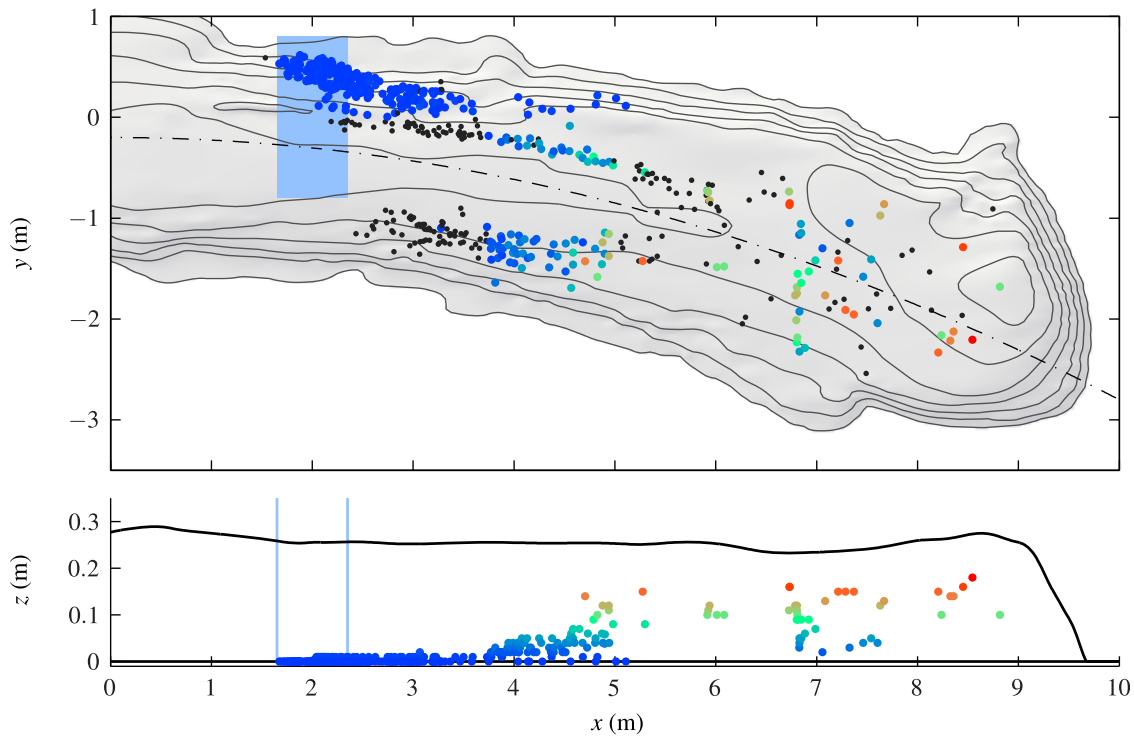


Figure 16. Positions of tracer pebbles in the August 27th deposit. Pebbles were initially distributed uniformly in a rectangular area (shaded blue) 2 m downstream of the flume exit. Pebbles are colored according to their height in the deposit; no heights were recorded for stones plotted in black. (top) In the overhead view, contours of deposit thickness are every 5 cm. The flow centerline is indicated by the dot-dashed line. (bottom) In the side view, the depth of the deposit along the centerline is indicated by the solid line. Note the $4.6 \times$ vertical exaggeration.

(0.0125–8 mm) volume fractions corresponding to large and small fractions respectively.

[49] The particle segregation and transport model of *Gray and Thornton* [2005] describes the time-evolution of the small-particle volume fraction ϕ^s (where $0 \leq \phi^s \leq 1$) in an

incompressible bi-disperse granular flow. The model equation can be written as

$$\frac{\partial \phi^s}{\partial t} + \frac{\partial}{\partial x}(\phi^s u) + \frac{\partial}{\partial y}(\phi^s v) + \frac{\partial}{\partial z}(\phi^s [w - q(1 - \phi^s)]) = 0, \quad (19)$$



Figure 17. Photograph of the 27th August deposit termination. A layer of coarse-enriched surface material approximately 5 cm thick has been removed from a sector of the deposit, uncovering two white tracer stones. White lines on the undisturbed deposit surface are topographic contours, determined by laser leveling and applied with paste.

where $\mathbf{u} = (u, v, w)$ is the prescribed bulk flow velocity field and q is the segregation rate. We use the velocity field \mathbf{u} , with a velocity profile corresponding to $\alpha = 0.5$, and a typical segregation rate of 0.035 m s^{-1} , inferred from the experimental flows in sections 3.2 and 5, respectively. The bracketed term $w - q(1 - \phi^s)$ in equation (19) corresponds to the vertical velocity of small particles. When $q = 0$ this term reduces to the bulk vertical velocity and the equation reduces to the tracer equation. In the case $\phi^s = 0$, the vertical velocity is simply $w - q$, representing a small particle descending through a bulk flow of pure large particles at a speed q . In this bi-disperse model the large-particle volume fraction is simply equal to $\phi^l = 1 - \phi^s$, and equation (19) can be rewritten in terms of this variable as

$$\frac{\partial \phi^l}{\partial t} + \frac{\partial}{\partial x}(\phi^l u) + \frac{\partial}{\partial y}(\phi^l v) + \frac{\partial}{\partial z}(\phi^l [w + q(1 - \phi^l)]) = 0. \quad (20)$$

The corresponding vertical velocity of large particles $w + q(1 - \phi^l)$ is equal to the bulk vertical velocity if $q = 0$. The case $\phi^l = 0$ represents a large particle rising through the bulk flow of pure small particles at speed q .

[50] *Gray and Thornton* [2005] show that this model predicts that the rise of large particles eventually leads to a surface layer composed entirely of large particles, which is separated from a region of small particles beneath by a sharp interface (a shock in particle concentration). When combined with a shearing flow in which material at the surface moves faster than that at the base, this layered structure leads to enhanced transport of large material toward the front of the flow. *Gray and Ancy* [2009] show that, in a two-dimensional granular avalanche, the segregation model predicts an accumulation of large particles at the flow front, which is separated from the flow behind by a lens-shaped region of mixed large and small particles known as a breaking size-segregation wave [*Thornton and Gray*, 2008]. The segregation occurring within the breaking size-segregation wave causes a recirculating region of large particles in the flow head, while small particles segregate downward and are transported away from the front.

[51] In real granular flows, large and small particles are rarely separated by a sharp interface owing to random fluctuation of the particles, which renders the interface diffuse. While this effect can be added to the segregation model by means of a diffusive remixing term [*Gray and Chugunov*, 2006], for simplicity we present the results below without diffusive remixing; the qualitative results are unchanged by the addition of small diffusion rates.

[52] We consider in particular the solution in the center plane $y = 0$ in the moving frame, indicated by black particle paths in Figure 12. On this plane the transverse velocity v' is zero, which means that y -derivatives of ϕ^s no longer appear in equation (19). The solution for ϕ^s on $y = 0$ therefore uncouples from the solution for $y \neq 0$, and equation (19) reduces to an equation in two spatial variables:

$$\frac{\partial \phi^s}{\partial t} + \frac{\partial}{\partial \xi}(\phi^s u') + \frac{\partial}{\partial z}(\phi^s [w' - q(1 - \phi^s)]) = -\phi^s \frac{\partial v'}{\partial y}. \quad (21)$$

where u' , w' , q and $\partial v'/\partial y$ are prescribed by the velocity field. The term on the right-hand side represents the flux of particles away from the flow centerline by the velocity gradient

$\partial v'/\partial y$. The boundary condition on ϕ^s is determined by the condition that no flux of particles occurs through the flow boundary. Since no diffusive remixing is included in equation (21), this condition implies that $\phi^s = 0$ or $\phi^s = 1$ [*Gray and Chugunov* 2006, equation 2.24]. We assume that particles in the flow far upstream of the front have segregated to form a layer of coarse material, taken to be 5 cm thick based on the experimental deposits (Figure 17), on top of a layer of fine material.

[53] The model predicts a pure coarse-particle layer on the surface of the flow which ‘wraps around’ the advancing flow front and creates a coarse-particle region at the base of the flow extending $\sim 0.8 \text{ m}$ behind the front (Figure 18a). In the interior of the flow a roughly elliptical region of mixed coarse and fine particles—a breaking size-segregation wave—extends from 0.3 m to 3.7 m behind the front. The coarse-rich front and surface layer and the breaking size-segregation wave resemble those found by *Gray and Ancy* [2009] for a two-dimensional avalanche.

[54] As in section 3.2, the velocity profile through the depth of the flow has material near the base of the flow moving more slowly than the advancing front, so that it moves backwards in the moving frame. Correspondingly, material near the surface moves faster than the front and so is transported forward. Coarse particles at the flow surface are transported forward and descend the rounded front of the flow to reach the base (Figure 18b). Here they are overpassed and are transported back away from the front, forming the coarse-particle layer at the flow base. As these coarse particles begin to re-segregate up through the flow, material at the flow base transitions from coarse-enriched near the front to coarse-depleted farther upstream. As the rising coarse particles reach the upper part of the flow, they are again transported toward the flow front but their segregation is stopped before they reach the flow surface by the coarse layer of particles occupying the top $\sim 5 \text{ cm}$ of the flow. The coarse-enriched surface layer effectively acts as a lid, preventing particles from segregating further.

[55] We compare the particle size-distributions measured on the center plane of the August 27th deposit (Figure 19) with the coarse and fine particle concentrations predicted by the model (Figure 18a). At 1.25 m and 0.55 m upstream of the deposit termination (Figure 19), coarse material is enriched both at the surface and base of the deposit, with no evidence of enrichment at samples taken from the middle of the deposit. This pattern is consistent with the surface and basal layers of coarse enrichment predicted by the segregation model at $\xi = -0.55 \text{ m}$ and $\xi = -1.25 \text{ m}$ (Figure 18a). There is a strong contrast between coarse-enriched top and bottom samples and the middle sample, which shows no such enrichment at 0.55 m upstream from the deposit termination, despite the deposit thickness being only 15 cm . This evidence implies that the thickness of the coarse-enriched layer is no larger than 5 cm , or approximately three coarse-particle diameters.

[56] In contrast to samples $\leq 1.25 \text{ m}$ upstream of the deposit termination, the surface $2.5\text{--}8 \text{ m}$ from the termination has lesser or no coarse enrichment; this difference is due to the rapid application of the flow diverter. After the diverter was brought down, the final surface particles to pass under it reached $x = 7.5 \text{ m}$ on the deposit axis, approximately 2.5 m upstream of the deposit termination. The coarse-

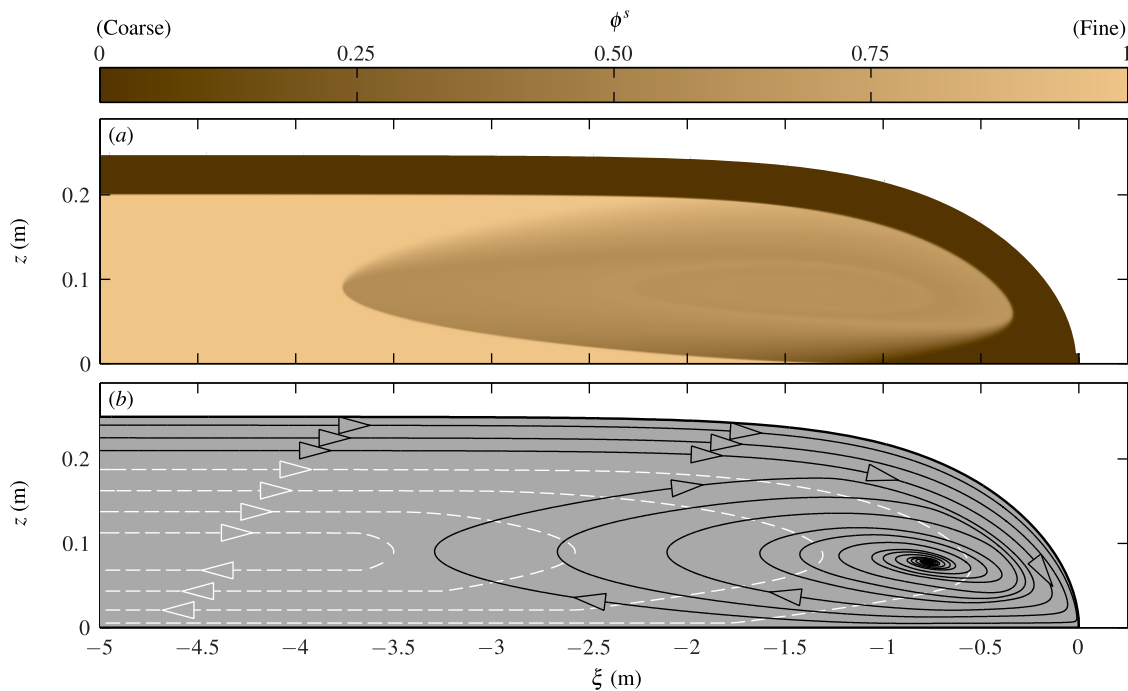


Figure 18. Solution of the segregation equation in the central plane of the debris-flow runout (equation (21)), with a velocity field inferred from the experimental flows. (a) Small-particle concentration ϕ^s ; (b) Paths of coarse particles (black lines) and fine particles (dashed white lines).

depleted material at the deposit surface upstream of $x = 7.5$ m therefore represents a combination of material beneath the flow surface, which was revealed when the flow continued to shear down-stream following the deployment of the flow diverter, and of debris that encroached under the diverter. The surface material within 1.25 m of the deposit termination was on the flow surface prior to the application of the diverter, and its strong coarse enrichment is consistent with a coarse layer covering the flow surface during the runout. In natural flows, and in experimental flows that are not diverted, we would expect to see the coarse-enriched surface layer extend much further than 1.25 m upslope of the deposit termination.

[57] Coarse particles at the base of the deposit are enriched within 2.5 m from the deposit termination, and coarse-depleted farther upstream. The farthest-downstream basal sample is the most strongly enriched (Figure 19), which reflects the model prediction that the basal coarse-particle layer originating at the flow front re-segregates upward as it is passed over by the flow. By 4 m upstream of the front, segregation has lifted coarse particles completely out of the basal layer (Figure 19), a distance consistent with the predicted size of the breaking size-segregation wave.

[58] The model prediction that coarse particles that re-segregate through the flow are prevented from segregating to the surface by a coarse-enriched surface layer is supported by the location in the deposit of the large tracer pebbles. The paths of the tracer pebbles, which were representative coarse particles introduced into the flow at the base of the flow front, directly correspond to the path through the flow taken by coarse particles that reached the flow front and were overpassed. The observed rise of these tracer pebbles to a maximum height of 5–10 cm below the

deposit surface (Figure 16) is consistent with the modelled upward movement of coarse particles and the halting of segregation by the overlying coarse-particle layer (Figure 18b).

7. Discussion

[59] In the three-dimensional debris-flow velocity field calculated in section 3.2, the mass fluxes entering and leaving the flow head were equal, due to the flow being incompressible and steady in the moving frame. The segregation model captures an important additional characteristic of the debris-flow runout: that the fluxes of both coarse or fine particles entering a region must each be balanced by a corresponding flux of coarse or fine particles leaving that region. Along the center-plane upstream of the flow head, the flow has three distinct layers: at the surface, coarse particles are advected toward the flow front; beneath these, fine particles are advected toward the flow front; and at the flow base, fine particles are advected away from the flow front (Figure 18b). In the center-plane, the fluxes in these three layers result in a net flux of material toward the flow front, which is balanced by the transverse flux of material away from the center-plane, $-\phi^s \partial v / \partial y$. These fluxes can be calculated from the solution of the segregation equations plotted in Figure 18. Of the fine material transported toward the front in the middle of the flow center-plane, 68% descends to the base and flows away from the head, following the dashed white lines in Figure 18b. The remainder of the fine material and all of the coarse surface material transported to the flow front are removed from the center-plane by the transverse flux. The composition of material leaving the center-plane through transverse shear is 78% coarse, a substantial coarse enrichment compared to the 28% coarse inflow flux. In

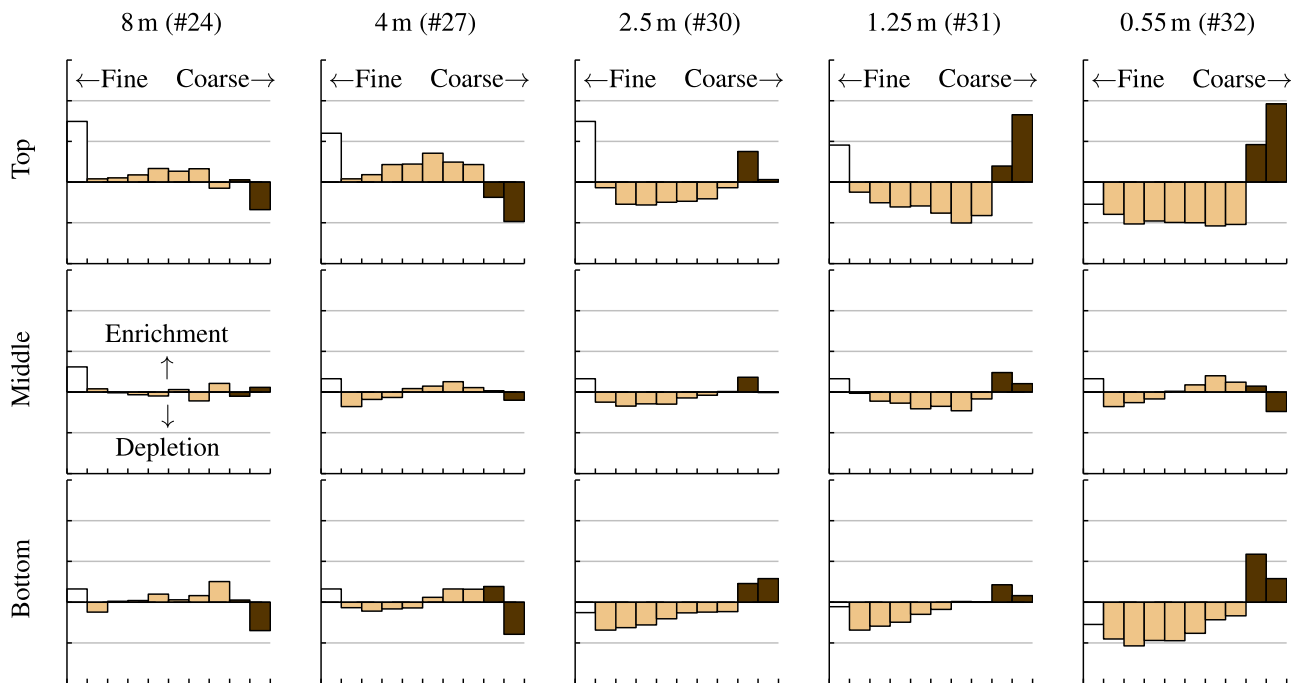


Figure 19. Relative abundance plots of deposit granulometry in the central channel of the 27th August experiment. Samples are labeled by their site number and by their distance upstream of the deposit termination at $x = 9.7$ m. Axes for the plots are as for Figure 13c.

summary, the model shows that of the material transported into the flow head, fine particles mostly leave the head at the base of the central channel, whereas coarse particles are transported outwards in a transverse direction into the levees.

[60] If the particle fluxes into and out of a flow region do not balance, a steady solution to the segregation equation cannot exist and the volume fraction of coarse and fine material within the flow evolves with time. This unsteady state occurs if the inflow of particles is sufficiently coarse that the flux of coarse particles entering the flow head is greater than that which can leave the head through transverse motion. In this situation, the segregation equation predicts that the flow head is composed of pure coarse particles, with the downstream length of the coarse-particle head growing in time. This solution neglects the feedback of such a coarse-particle-enriched head on the bulk velocity field; in natural debris flows, the growing resistance to flow of the coarse-enriched head is likely to slow and block the flow behind [Iverson, 1997; Major and Iverson, 1999]. This blockage is likely to cause a breakout of the channelized flow through existing emplaced levees or the splitting of a single leveed channel into two, or it may simply halt the flow. The formation of fingered deposits with a lobe-and-cleft morphology, as compared to elongated leveed channel deposits, may therefore indicate a greater flux of coarse levee-forming clasts to the flow front.

[61] Solutions of the segregation model in a two-dimensional flow also exhibit a steady or a growing coarse-particle head [Gray and Ancey, 2009]. While enhanced transport of coarse material in the surface-layer to the flow front still occurs in a two-dimensional flow, the flow is uniform in the transverse direction, implying that $\partial v/\partial y = 0$

and that there is no transverse flux of material out of the flow head. This results in a growing coarse-particle head, which is captured by the depth-integrated size segregation model of Gray and Kokelaar [2010a, 2010b]. In small-scale two-dimensional avalanche experiments, a coarse-particle layer is deposited at the flow base [Gray and Ancey, 2009]. Adding deposition to the segregation model allows deposited coarse particles to leave the head at the base of the flow and allows a steady solution to be found [Gray and Ancey, 2009], analogous to the way in which the transverse flux of coarse material out of the head allows a steady solution in a three-dimensional avalanche. The large-scale debris-flow experiments described in this paper indicate that in an unconfined debris flow, the primary deposition of coarse particles is in lateral levees, rather than at the flow base.

[62] The solutions to the segregation equation in a shearing granular avalanche, both in the two-dimensional depositing flow and in the center-plane of the three-dimensional solution presented here, contain a breaking size-segregation wave close to the flow front. In two dimensions, large particles recirculate within this breaking size-segregation wave, following closed streamlines [Gray and Ancey, 2009]. In the three-dimensional velocity field, Figure 18b indicates that the coarse particles instead spiral inward to a stagnation point within the breaking size-segregation wave, where coarse particles on the centerline become stationary in the moving frame. In this region, the outward-directed transverse velocity components advect material that is not exactly on the flow center-plane out toward the flow margins.

[63] A typical trajectory of a coarse particle through the flow illustrates the mechanisms pertinent to the formation of coarse-particle-rich levees (Figure 20). Particle size-segregation causes a coarse particle in the channel to rise to

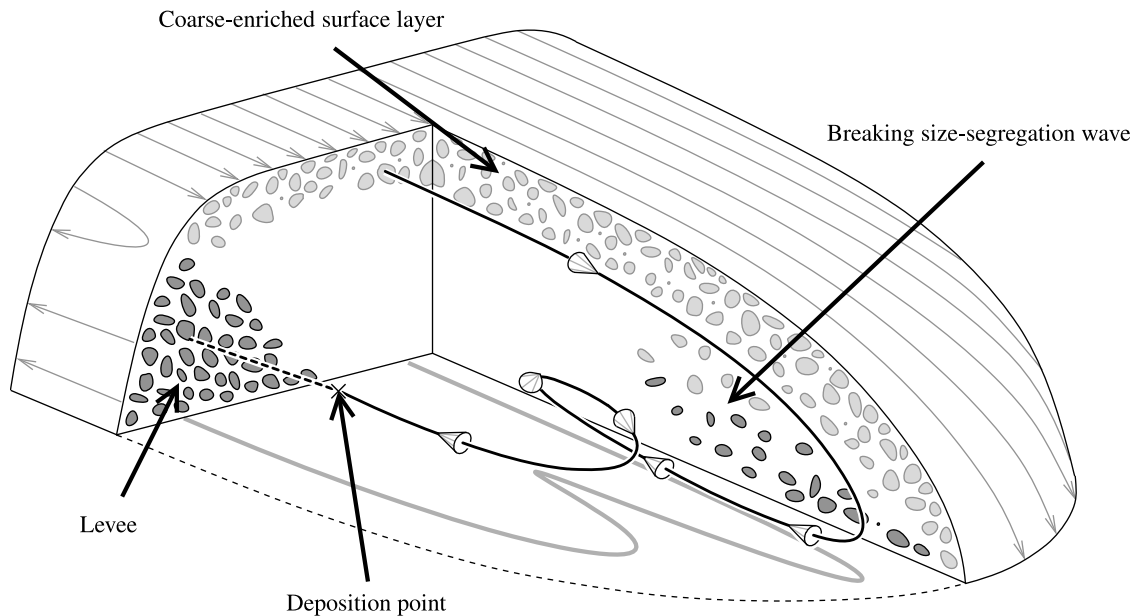


Figure 20. Cutaway sketch showing a moving-frame view of the coarse-enriched regions and the three-dimensional path of a segregating coarse particle through the debris-flow head. Coarse particles with light shading are those moving downstream faster than (and therefore toward) the flow front. Coarse particles with darker shading are stationary or moving slower than the flow front; these include those in the levees and near the base of the flow. The path of a typical coarse particle in the surface layer near the center of the flow is shown. The particle is transported into the flow head and is overpassed when it reaches the flow boundary. Now at the base of the flow, it moves more slowly than the advancing flow front, and begins to segregate upwards as part of a breaking size-segregation wave. The particle may recirculate a number of times within the flow head, but is continually advected away from the flow centerline, toward the sides of the flow. The particle deposits when it becomes part of the progressively accreting levees.

near the flow surface, where velocities greater than the average transport it to the flow head. If the particle is sufficiently close to the flow axis it reaches the flow front, where it migrates to the base of the flow and is then overpassed (Figure 8). The particle may again segregate upwards until it reaches the coarse-enriched layer covering the flow surface, and then recirculate within the flow head. During recirculation, material is advected away from the flow center-plane by the transverse component of the velocity. In the moving frame, coarse particles therefore follow helical spiral trajectories within the flow head and move progressively farther toward the flow margins (Figure 20). Near the flow margins, particles throughout the depth of the flow move more slowly than the flow front (as indicated by the pink shading in Figure 12). When a coarse particle is advected into this region, it ceases recirculation and is left behind by the advancing flow front. As it moves out of the flow head, the particle reaches the deposition surface of the progressively accreting levee and comes to rest.

[64] The experimental debris flows presented here are composed of grains ranging from 0.0625 mm to 32 mm, roughly 15% of the typical flow height. This is in contrast to some natural debris flows, which have a much wider grain size distribution, ranging from clay particles to boulders as large as the flow height itself. Evidence from experimental debris flows with a wider grain size distribution suggests that the mechanism of levee formation presented in this paper is not hindered by the presence of larger or smaller

grains. Experimental debris flows with an increased proportion of very fine particles ($d < 0.0625$ mm comprising 7% by mass) exhibit very similar levee formation processes to those seen in the experiments presented here [Iverson *et al.*, 2010], although liquefaction of the muddy core of the flow persists for longer when a greater fraction of mud is present, enabling the flow to run out further. Similarly, in experiments in which rocks of diameter 10 cm are added to the sediment mixture, levees composed of both coarse material and rocks are formed by a similar process. A prerequisite for the levee formation process (Figure 20) is particle-size segregation. For the smallest and largest grains in a flow, particle-size segregation may be hindered, through particles being suspended in the interstitial fluid or through being too heavy to be lifted by the surrounding grains, respectively. While these fractions would not form levees through the same process, particles of intermediate grain size are likely to segregate and form levees, as described in this paper.

[65] The kinematic balance of coarse particles through the flow head allows the formation of coarse-enriched levees to be linked directly to the enhanced transport of coarse material in the channelized flow behind. Similarly, the dynamic balance of downstream momentum in the flow head can be used to infer dynamical constraints on levee-channelized flows. In a steadily propagating flow, the basal friction resisting the motion of the flow head is balanced by pressure at the back of the head, a gravitational body force (for flows propagating downslope) and by the advection of momentum into the head from the trailing, low-friction part of the flow.

This advection force is due to the transport of material through the flow head shown in Figure 9b. The transport of material through the flow head is therefore important not only in the kinematics of levee formation, but also through its contribution to flow mobility. The momentum advection pressure scales like $u(u - u_F)$, or the square of the Froude number times the pressure term. For supercritical flows propagating on shallow inclines, such as the experimental debris-flow runouts presented here, the advection of momentum into the head is therefore the a major contributor to the flow mobility.

[66] On a constant incline, the steady propagation of the flow, resulting from the force balance in the head, will continue as long as the advection of momentum into the head is maintained from the channelized material behind. Thus, on a slope sufficiently steep to support a steady uniform flow of the low-friction material in the channel, steady propagation of the considerably more frictional flow head is attained, with the consequent deposition of frictional levees. The complementary roles of the flow head and trailing channelized flow, both in the flow kinematics and dynamics, emphasize the crucial importance of the head-and-tail architecture in debris flows [Iverson, 1997]. A model that combines these dynamic, kinematic and size-segregation processes could represent a significant theoretical advance, and might be achieved by augmenting existing depth-averaged geophysical mass flow models [e.g., Savage and Hutter, 1989; Iverson, 1997; Gray et al., 1999; Iverson and Denlinger, 2001; Gray et al., 2003; Johnson and Gray, 2011] with a depth-averaged kinematic segregation model [Gray and Kokelaar, 2010a, 2010b].

8. Conclusion

[67] Coarse-particle-rich levees formed in our debris-flow experiments by rapid progressive streamwise accretion. A model for their formation includes both upward segregation of coarse particles and shear within the flow, which cause enhanced transport of coarse material to the flow front. A diverging transverse velocity field in the head then transports this coarse material to the flow margins, where it deposits as lateral levees.

[68] Each stage in the levee-formation process was directly observed in our experiments. Size-segregation was measured using coarse tracer particles, which rise at a typical rate of 3.5 cm s^{-1} , about 1% of the typical speed of the channelized flow, $\sim 4 \text{ m s}^{-1}$. This segregation rate is sufficient to cause a substantial coarse enrichment of the upper part of the flow. We inferred shear with depth within the flow from measurements of the surface velocity field and front propagation rate, and from direct observations of surface particles being advected to the advancing flow margin and transferred to the base of the flow. The surface velocity field (Figure 9) demonstrates that the lateral transport of material from the central channel into the levees occurs entirely within the flow head.

[69] The mechanisms governing this motion of the coarse particles through the flow head to form coarse-enriched levees have been demonstrated in debris-flow experiments but are generic to a wide variety of geophysical and grain flows. The kinematic nature of the model presented here means that the mechanism for levee formation depends only

on particle size-segregation and the flow velocity field. The model therefore has the potential to describe the formation of coarse-particle levees in debris flows, pyroclastic density currents [Branney and Kokelaar, 2002; Félix and Thomas, 2004] and snow avalanches [Gray and Kokelaar, 2010a, 2010b], despite the wide variety of mechanisms that govern the complex and spatially varying rheology of these flows [Iverson and Vallance, 2001].

[70] **Acknowledgments.** We gratefully acknowledge the experimental assistance provided by A. Thornton, J. Griswold, K. Swinford and D. George, and thank J. Vallance and C. Ancey for helpful reviews of the manuscript. Nico Gray, Peter Kokelaar and Anthony Thornton were supported by NERC grant NE/E003206/1, and Nico Gray additionally by an EPSRC Advanced Research Fellowship (GR/S50052/01 and GR/S50069/01) as well as EP/I019189/1 Critical Phenomena and Collective Behaviour of MultiParticle Complex Systems. Chris Johnson acknowledges support from NERC DTG NE/G523747/1 and an EPSRC DTA.

References

- Bagnold, R. A. (1954), Experiments on a gravity-free dispersion of large solid spheres in a Newtonian fluid under shear, *Proc. R. Soc. A*, 225(1160), 49–63, doi:10.1098/rspa.1954.0186.
- Bartelt, P., and B. W. McArdell (2009), Granulometric investigations of snow avalanches, *J. Glaciol.*, 55(193), 829–833, doi:10.3189/002214309790152384.
- Batchelor, G. K. (1967), *An Introduction to Fluid Dynamics*, Cambridge Univ. Press., Cambridge, U. K.
- Branney, M. J., and B. P. Kokelaar (2002), *Pyroclastic Density Currents and the Sedimentation of Ignimbrites*, *Geol. Soc. Mem.*, vol. 27, Geol. Soc., London.
- Calder, E. S., R. S. J. Sparks, and M. C. Gardeweg (2000), Erosion, transport and segregation of pumice and lithic clasts in pyroclastic flows inferred from ignimbrite at Lascar Volcano, Chile, *J. Volcanol. Geotherm. Res.*, 104(1–4), 201–235, doi:10.1016/S0377-0273(00)00207-9.
- Conway, S. J., A. Decaulne, M. R. Balme, J. B. Murray, and M. C. Towner (2010), A new approach to estimating hazard posed by debris flows in the Westfjords of Iceland, *Geomorphology*, 114(4), 556–572, doi:10.1016/j.geomorph.2009.08.015.
- Denlinger, R. P., and R. M. Iverson (2004), Granular avalanches across irregular three-dimensional terrain: 1. Theory and computation, *J. Geophys. Res.*, 109, F01014, doi:10.1029/2003JF000085.
- Dolgunin, V. N., and A. A. Ukolov (1995), Segregation modelling of particle rapid gravity flow, *Powder Technol.*, 83(2), 95–103, doi:0032-5910(94)02954-M.
- Félix, G., and N. Thomas (2004), Relation between dry granular flow regimes and morphology of deposits: formation of levées in pyroclastic deposits, *Earth Planet. Sci. Lett.*, 221(1–4), 197–213, doi:10.1016/S0012-821X(04)00111-6.
- Golick, L. A., and K. E. Daniels (2009), Mixing and segregation rates in sheared granular materials, *Phys. Rev. E*, 80, 042301, doi:10.1103/PhysRevE.80.042301.
- Gray, J. M. N. T., and C. Ancey (2009), Segregation, recirculation and deposition of coarse particles near two-dimensional avalanche fronts, *J. Fluid Mech.*, 629, 387–423, doi:10.1017/S0022112009006466.
- Gray, J. M. N. T., and C. Ancey (2011), Multi-component particle size segregation in shallow granular avalanches, *J. Fluid Mech.*, 678, 535–588, doi:10.1017/jfm.2011.138.
- Gray, J. M. N. T., and V. A. Chugunov (2006), Particle-size segregation and diffusive remixing in shallow granular avalanches, *J. Fluid Mech.*, 569, 365–398, doi:10.1017/S0022112006002977.
- Gray, J. M. N. T., and B. P. Kokelaar (2010a), Large particle segregation, transport and accumulation in granular free-surface flows, *J. Fluid Mech.*, 652, 105–137, doi:10.1017/S002211201000011X.
- Gray, J. M. N. T., and B. P. Kokelaar (2010b), Large particle segregation, transport and accumulation in granular free-surface flows—Erratum, *J. Fluid Mech.*, 657, 539, doi:10.1017/S0022112010003241.
- Gray, J. M. N. T., and A. R. Thornton (2005), A theory for particle size segregation in shallow granular free-surface flows, *Proc. R. Soc. A*, 461(2057), 1447–1473, doi:10.1098/rspa.2004.1420.
- Gray, J. M. N. T., M. Wieland, and K. Hutter (1999), Free surface flow of cohesionless granular avalanches over complex basal topography, *Proc. R. Soc. A*, 455(1985), 1841–1874, doi:10.1098/rspa.1999.0383.
- Gray, J. M. N. T., Y. C. Tai, and S. Noelle (2003), Shock waves, dead zones and particle-free regions in rapid granular free-surface flows, *J. Fluid Mech.*, 491, 161–181, doi:10.1017/S0022112003005317.

- Heim, A. (1932), *Bergsturz und Menschenleben*, Fretz and Wasmuth, Zürich, Switzerland.
- Hoblitt, R. P. (1986), Observations of the eruptions of July 22 and August 7, 1980, at Mount St. Helens, Washington, *U.S. Geol. Surv. Prof. Pap.*, 1250, 44 pp.
- Iverson, R. M. (1997), The physics of debris flows, *Rev. Geophys.*, 35(3), 245–296, doi:10.1029/97RG00426.
- Iverson, R. M., and R. P. Denlinger (2001), Flow of variably fluidized granular masses across three-dimensional terrain: 1. Coulomb mixture theory, *J. Geophys. Res.*, 106(B1), 537–552, doi:10.1029/2000JB900329.
- Iverson, R. M., and J. W. Vallance (2001), New views of granular mass flows, *Geology*, 29(2), 115–118, doi:10.1130/0091-7613(2001)029<0115: NVOGMF>2.0.CO;2.
- Iverson, R. M., M. Logan, R. G. LaHusen, and M. Berti (2010), The perfect debris flow? Aggregated results from 28 large-scale experiments, *J. Geophys. Res.*, 115, F03005, doi:10.1029/2009JF001514.
- Johnson, A. M. (1965), A model for debris flow, Ph.D. thesis, Pa. State Univ., University Park.
- Johnson, A. M. (1970), *Physical processes in geology*, W. H. Freeman, New York.
- Johnson, A. M., and J. R. Rodine (1984), Debris flow, in *Slope Instability*, edited by D. Brunsten and D. B. Prior, pp. 257–361, John Wiley, New York.
- Johnson, C. G., and J. M. N. T. Gray (2011), Granular jets and hydraulic jumps on an inclined plane, *J. Fluid Mech.*, 675, 87–116, doi:10.1017/jfm.2011.2.
- Major, J. J. (1997), Depositional processes in large-scale debris-flow experiments, *J. Geol.*, 105(3), 345–366, doi:10.1086/515930.
- Major, J. J., and R. M. Iverson (1999), Debris-flow deposition: Effects of pore-fluid pressure and friction concentrated at flow margins, *Geol. Soc. Am. Bull.*, 111(10), 1424–1434, doi:10.1130/0016-7606(1999)111<1424:DFDEOP>2.3.CO;2.
- Mangold, N., A. Mangeney, V. Migeon, V. Ansan, A. Lucas, D. Baratoux, and F. Bouchut (2010), Sinuous gullies on Mars: Frequency, distribution, and implications for flow properties, *J. Geophys. Res.*, 115, E11001, doi:10.1029/2009JE003540.
- Middleton, G. V. (1970), Experimental studies related to problems of flysch sedimentation, in *Flysch Sedimentology in North America*, edited by J. Lajoie, *Geol. Assoc. Can. Spec. Pap.*, 7, 253–272.
- Middleton, G. V., and M. A. Hampton (1976), Subaqueous sediment transport and deposition by sediment gravity flows, in *Marine Sediment Transport and Environmental Management*, edited by D. J. Stanley and D. J. P. Swift, pp. 197–218, John Wiley, New York.
- Pierson, T. (1986), Flow behavior of channelized debris flows, Mount St. Helens, Washington, in *Hillslope Processes*, edited by A. D. Abrahams, pp. 269–296, Allan and Unwin, Boston, Mass.
- Pouliquen, O., and J. W. Vallance (1999), Segregation induced instabilities of granular fronts, *Chaos*, 9, 621–630, doi:10.1063/1.166435.
- Pouliquen, O., J. Delour, and S. B. Savage (1997), Fingering in granular flows, *Nature*, 386, 816–817, doi:10.1038/386816a0.
- Rowley, P. D., M. A. Kuntz, and N. S. MacLeod (1981), Pyroclastic flow deposits, in *The 1980 Eruptions of Mount St. Helens, Washington*, edited by P. W. Lipman and D. R. Mullineaux, *U.S. Geol. Surv. Prof. Pap.*, 1250, 489–512.
- Savage, S. B., and K. Hutter (1989), The motion of a finite mass of granular material down a rough incline, *J. Fluid Mech.*, 199, 177–215, doi:10.1017/S0022112089000340.
- Savage, S. B., and C. K. K. Lun (1988), Particle size segregation in inclined chute flow of dry cohesionless granular solids, *J. Fluid Mech.*, 189, 311–335, doi:10.1017/S002211208800103X.
- Sharp, R. P., and L. Nobles (1953), Mudflow of 1941 at Wrightwood, southern California, *Geol. Soc. Am. Bull.*, 64(5), 547–560, doi:10.1130/0016-7606(1953)64[547:MOAWSC]2.0.CO;2.
- Shearer, M., J. M. N. T. Gray, and A. R. Thornton (2008), Stable solutions of a scalar conservation law for particle-size segregation in dense granular avalanches, *Eur. J. Appl. Math.*, 19, 61–86, doi:10.1017/S0956792507007280.
- Sparks, R. (1976), Grain size variations in ignimbrites and implications for the transport of pyroclastic flows, *Sedimentology*, 23(2), 147–188, doi:10.1111/j.1365-3091.1976.tb00045.x.
- Stiny, J. (1910), *Die Muren*, Verl. der Wagnerischen Univ.-Buchhandl., Innsbruck, Austria, doi:10.1111/j.1365-3091.1976.tb00045.x.
- Thornton, A. R., and J. M. N. T. Gray (2008), Breaking size segregation waves and particle recirculation in granular avalanches, *J. Fluid Mech.*, 596, 261–284, doi:10.1017/S0022112007009445.
- Thornton, A. R., J. M. N. T. Gray, and A. J. Hogg (2006), A three-phase mixture theory for particle size segregation in shallow granular free-surface flows, *J. Fluid Mech.*, 550, 1–25, doi:10.1017/S0022112005007676.
- Vallance, J. W., and S. B. Savage (2000), Particle segregation in granular flows down chutes, in *IUTAM Symposium on Segregation in Granular Flows*, edited by A. D. Rosato and D. L. Blackmore, pp. 31–52, Kluwer Acad., Boston, Mass.
- Wiederseiner, S., N. Andreini, G. Epely-Chauvin, G. Moser, M. Monnereau, J. M. N. T. Gray, and C. Ancey (2011), Experimental investigation into segregating granular flows down chutes, *Phys. Fluids*, 23, 013301, doi:10.1063/1.3536658.
- Wilson, L., and J. W. Head (1981), Morphology and rheology of pyroclastic flows and their deposits, and guidelines for future observations, in *The 1980 Eruptions of Mount St. Helens, Washington*, edited by P. W. Lipman and D. R. Mullineaux, *U.S. Geol. Surv. Prof. Pap.*, 1250, 513–524.

J. M. N. T. Gray, School of Mathematics and Manchester Centre for Nonlinear Dynamics, Oxford Rd., University of Manchester, Manchester M13 9PL, UK.

R. M. Iverson, R. G. LaHusen, and M. Logan, Cascades Volcano Observatory, U.S. Geological Survey, Vancouver, WA 98683, USA.

C. G. Johnson, Department of Mathematics, University of Bristol, University Walk, Bristol BS8 1TW, UK. (chris.johnson@bristol.ac.uk)

B. P. Kokelaar, Department of Earth Sciences, University of Liverpool, Liverpool L69 3GP, UK.